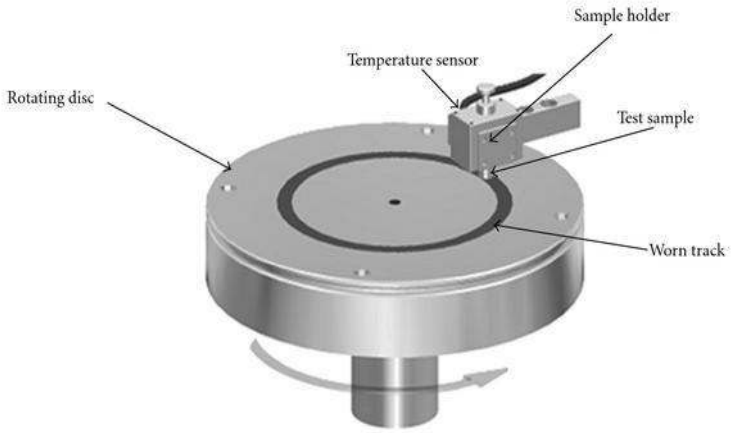

Chapter 6

Wear and Deformation Characteristics of Fe-Al_2O_3 Metal Matrix Nanocomposites

Chapter 6
Wear and Deformation Characteristics of Fe-Al_2O_3 Metal Matrix Nanocomposites

The present chapter describes the Wear and Deformation Characteristics of Fe-Al_2O_3 Metal Matrix Nanocomposites. The current chapter is divided into three sections.

Section 1: Wear behavior of Fe based Metal Matrix Nanocomposites reinforced with 5% Al_2O_3 sintered in an argon atmosphere in the temperature range 900°C - 1100°C for 1 - 3 hours. In order to study the type of wear mechanism, SEM images of the worn specimens were also observed.

Section 2: Wear Behavior of 10% Al_2O_3 reinforced specimen sintered in an argon atmosphere in the temperature range 900°C - 1100°C for 1 - 3 hours. For studying the type of wear mechanism, SEM images of the worn specimens were also analyzed.

Section 3: Deformation behavior of Fe -5% Al_2O_3 nanocomposites prepared by sintering at 1100^{o}C for 1 hour has been described in third section. The specimens were tested under different interfacial frictional conditions viz dry, solid lubricating and liquid lubricating. It also includes microstructural characterization of un-deformed and deformed specimens using scanning electron microscopy.

6.1 Wear Behavior of Fe-5% Al_2O_3 metal matrix nanocomposites

Wear behavior has been investigated using Pin on Disc Wear and Friction Testing Machine. The dry sliding wear tests of the synthesized nanocomposite specimens were carried out at a load of 0.5, 1.0 and 2.0 kg with sliding speed of 4 m/sec and sliding distance of 14.4 km covered in 1 hour as described in chapter 4.

6.1.1 Dry Sliding Wear Characterization

The dry sliding wear test of each specimen was carried out twice under identical wear test parameters. With these test results, average wear rate was determined and an error bar has been put at each value obtained. Table 6.1 shows wear rate (mm^3/km) for different specimens at different loads for Fe-5% Al_2O_3 MMNC system. Except for specimen 5AFe900(1) wear rate is less than 1 mm^3/km. This specimen has lowest densification and minimum formation of iron aluminate phase. Fig. 6.1 shows the wear rate (mm^3/km) vs. load plots for the specimens 5AFe900(1); 5AFe900(2) and 5AFe900(3) sintered at 900°C for 1-3 hours.

Table 6.1 Wear rate at different loads for Fe-5% Al_2O_3 specimens

S. No.	Specimen Code	Wear Rate (mm^3/km) at 0.5 kg Load	Wear Rate (mm^3/km) at 1.0 kg Load	Wear Rate (mm^3/km) at 2.0 kg Load
1	5AFe900(1)	0.1290	0.3014	1.1406
2	5AFe900(2)	0.0839	0.1566	0.6427
3	5AFe900(3)	0.1330	0.1895	0.5530
4	5AFe1000(1)	0.1445	0.2062	0.5197
5	5AFe1000(2)	0.0965	0.2238	0.5626
6	5AFe1000(3)	0.1166	0.1717	0.4890
7	5AFe1100(1)	0.1013	0.1652	0.4738
8	5AFe1100(2)	0.1825	0.2321	0.6630
9	5AFe1100(3)	0.0969	0.2898	0.5759

It is observed from Fig. 6.1 that the amount of the wear increases as we increase the load on the test rig from 0.5 kg to 2.0 kg. Specimens sintered at 900°C for 2h shows a small amount of wear at 0.5 kg and 1.0 kg load whereas the wear increases abruptly for a load of 2.0 kg.

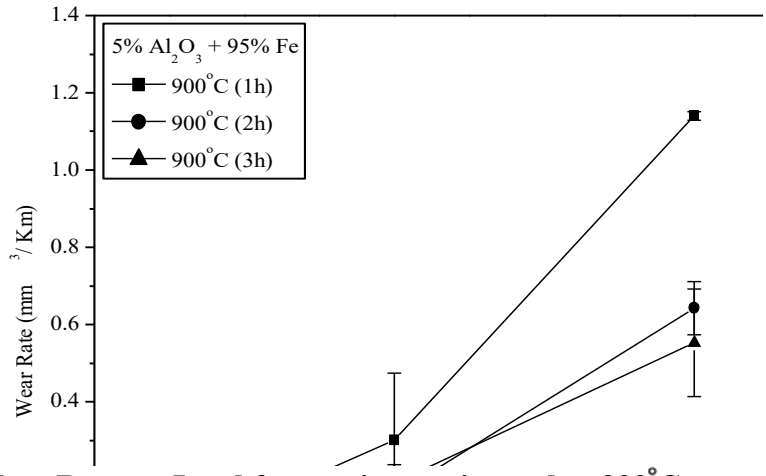

Fig. 6.1 Wear Rate vs. Load for specimens sintered at 900°C

The amount of wear for the specimens sintered at 900°C for 3h at 0.5 kg load is almost the same as the wear of the specimen sintered for 1h. At 1.0 kg load, the wear of the specimen sintered at 900°C for 3h is almost equal to that of the specimen sintered at 900°C for 2h. However, the amount of wear for the specimen sintered for 3h and carried out at 2.0 kg load is lowest as compared to the values of the wear for specimens sintered for 1h and 2h respectively.

Fig. 6.2 shows the wear rate vs. load plots for the specimens 5AFe1000(1); 5AFe1000(2) and 5AFe1000(3). The amount of wear from the specimens sintered for 1h, 2h and 3h at 1000°C is almost the same and its values are less as compared to the specimens sintered at 900°C. Similarly Fig. 6.3 shows the wear rate vs. load plot for specimens 5AFe1100(1); 5AFe1100(2) and 5AFe1100(3). For the specimen 5AFe1100(1), when the test is carried out at 0.5 kg load, a small amount of wear is found. On increasing the load from 1.0 kg to 2.0 kg, the amount of wear increased significantly.

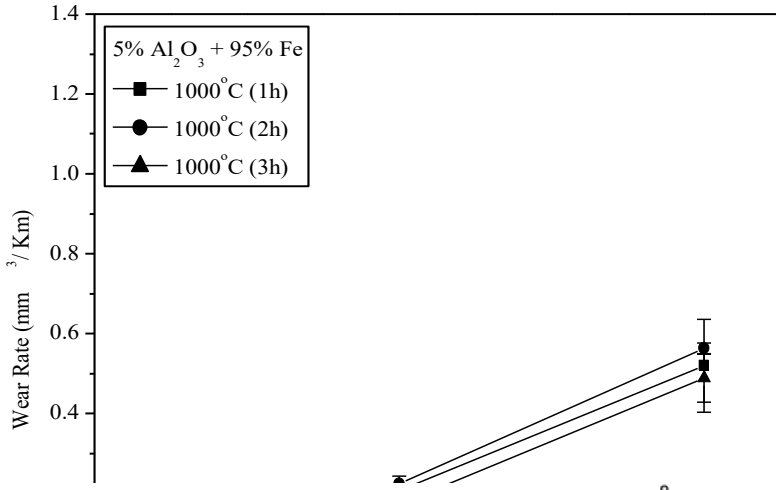

Fig. 6.2 Wear Rate vs. Load for specimens sintered at 1000°C

Similarly for 5AFe1100(2) wear increased on increasing the load as compared to the specimen 5AFe1100(1). Specimen 5AFe1100(3) did not show change in the wear rate at 0.5 kg load as compared to the specimen 5AFe1100(1). Under 1.0 kg load, its wear rate is highest. At 2.0 kg load the wear rate is intermittent between the wear rate for the specimen 5AFe1100(1) and 5AFe1100(2). From the Figs. 6.2 and 6.3 and Table 6.1 it can be seen that the wear rate is very less dependent on sintering temperature and time for specimens sintered at 1000 and 1100°C. At lower loads viz. 0.5 kg, the average wear rate is 0.1200 mm^3/km. It increases almost linearly with increasing load upto 2.0 kg having average value 0.55 mm^3/km. The specimens sintered at 900°C sintered for longer duration of time also behave similarly. These results are in conformity with the results of density and hardness on these nanocomposites. The specimens with optimum densification and hardness show low wear rate. Wear rate increases with increasing loads.

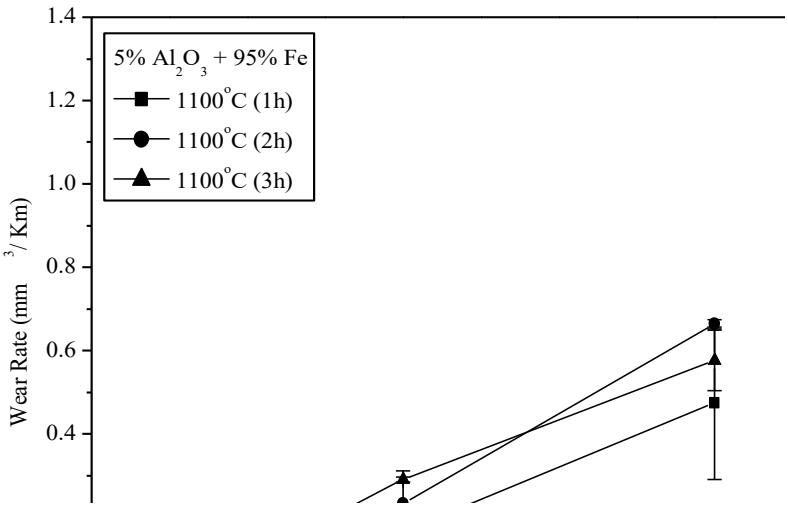

Fig. 6.3 Wear Rate vs. Load for specimens sintered at 1100°C

6.1.2 Scanning Electron Micrographs of worn specimens

Microstructural investigations of the worn surfaces of specimens help us to understand the nature of wear or wear mechanism and extent of damage to the surface after wear. Worn surface were examined with scanning electron microscope under low magnification (500X) as well as at high magnifications (5000X & 10000X). Microstructures were recorded for specimens which were tested at 2.0 kg load. Figures 6.4 to 6.8 show the microstructures of worn surfaces of representative MMNC specimens containing 5wt% Al_2O_3 worn out at 2 kg load for 1h interval. Fig. 6.4(a) shows the SEM micrograph of the specimen 5AFe900(2) at 200X which shows the uneven surface indicating the removal of the material as observed in materials with adhesive wear [Straffelini et al. (2004)]. These marks are small in size i.e. the peeling off the material due to adhesive wear could not extend over large part due to presence of ceramic reinforcements. Although the material is removed from the

surface due to wear, the surface of the material is not damaged. Large areas of specimens have smooth surface finish. Figs. 6.4(b) and 6.4(c) show the microstructure of the same specimen at 5000X and 10000X magnifications respectively. These show magnified wear marks indicating their depth and revealing that there are basically three types of the particles: black grains are of iron (Fe); white are of aluminum oxide (Al_2O_3) and the third one grey which are of iron aluminate ($FeAl_2O_4$). High magnification micrograph reveals internal microstructure of the specimens more clearly. It confirms that grains are nano size. These also show that the grains are not very much strongly bonded with each other due to lower sintering temperature and time in comparison to those which are sintered at higher temperatures and longer duration of time.

Fig. 6.5(a) shows the SEM micrograph of the specimen 5AFe900(3) at 200X which shows the generation of light wear marks on the specimen surface which are parallel to the sliding direction. The scoring marks indicate the removal of the material as observed in the materials with adhesive wear. These marks are small in size i.e. the peeling off the material due to adhesive wear could not extend over large part due to presence of ceramic reinforcements. There is a removal of the material from its surface but there is no damage to the surface. Large areas of specimens also show smooth surface finish. Figs. 6.5(b) and 6.5(c) show the microstructure of the same specimen at 5000X and 10000X magnifications respectively. These show magnified wear marks indicating their depth and revealing that there are basically three types of the particles: black grains are of iron (Fe); white are of aluminum oxide (Al_2O_3) and the third one grey which are of iron aluminate ($FeAl_2O_4$). In this specimen high magnification microstructure show better bonding between different grains. The damage to surface due to wear is also smaller.

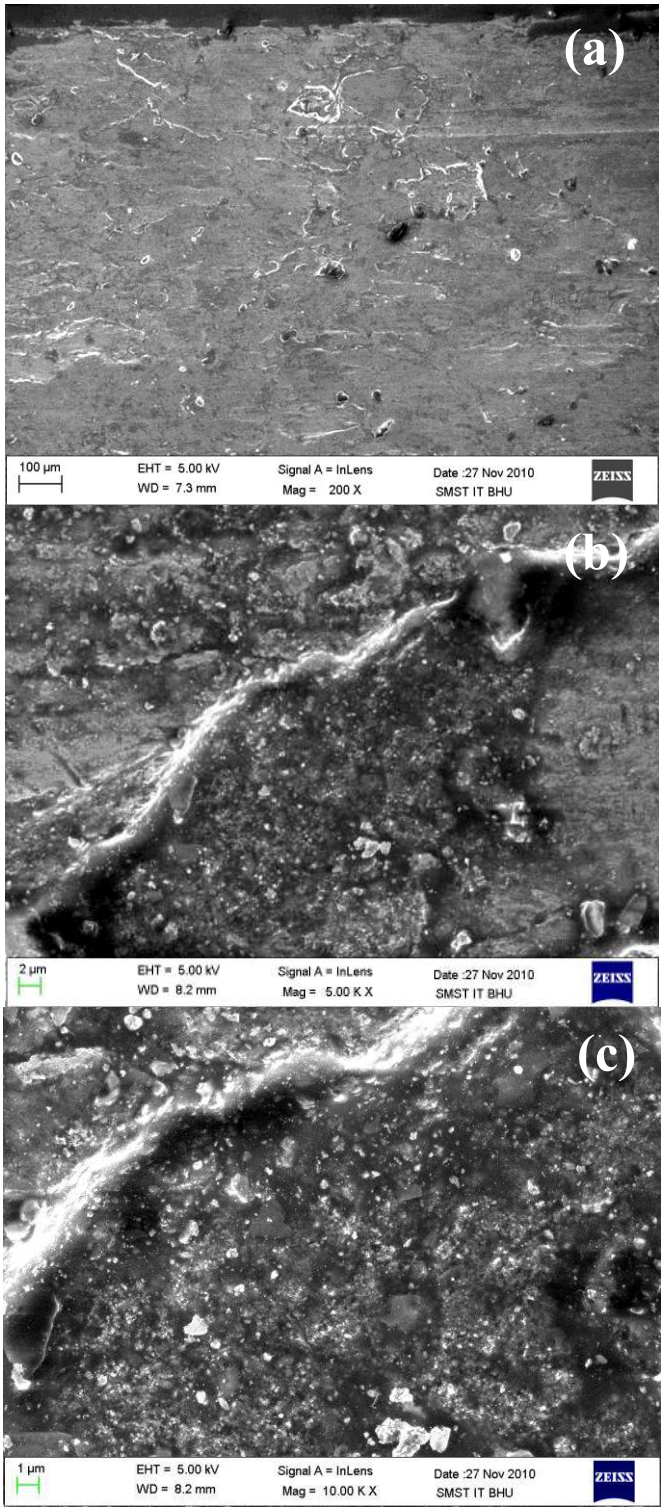

Fig. 6.4 SEM micrograph of 5AFe900(2) (a) 200X (b) 5000X and (c) 10000X magnification after measurement at 2 kg load

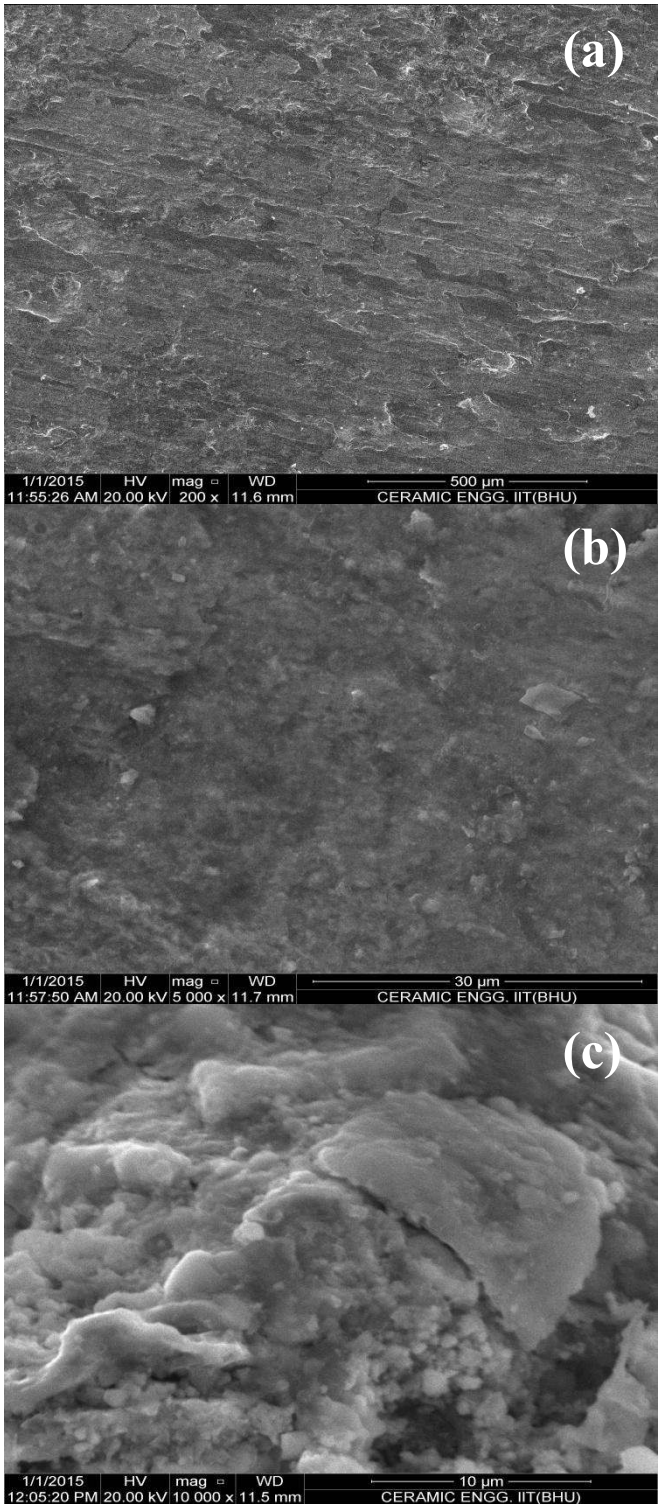

Fig. 6.5 SEM micrograph of 5AFe900(3) (a) 200X (b) 5000X and (c) 10000X magnification after measurement at 2 kg load

Fig. 6.6(a) shows the SEM micrograph of the specimen 5AFe1000(3) at 200X which shows light wear marks along with the generation of discernible layer of transferred material. The same micrograph also shows some scoring marks due to which there are some uneven patches generated over the entire surface of the specimen. The marks generated on the specimen surface are less severe in comparison to the specimen 5AFe900(3). These features suggest that adhesive wear was operative and its severity intensified with the progress in the time interval. Figs. 6.6(b) and 6.6(c) show the microstructure of the same specimen at 5000X and 10000X magnifications respectively. The micrograph shows the eroded surface of the specimen. The focused surface mainly shows the presence of the iron, alumina and iron aluminate phases respectively. SEM image also shows the iron aluminate particles which are mainly present on the periphery of the iron.

Fig. 6.7(a) shows the SEM micrograph of the specimen 5AFe1100(1) at 200X which shows the light scoring marks generated over the entire surface of the specimen. The same micrograph shows that there is polishing effect generated over the entire surface of the specimen. Adhesive wear is found in the present specimen. Due to the adhesive wear there is not damage to the surface of the specimen. Figs. 6.7(b) and 6.7(c) show the microstructure of the same specimen at 5000X and 10000X magnifications respectively. The micrograph shows the eroded surface of the specimen. The focused surface mainly shows the presence of the grains of iron, alumina and iron aluminate. Nano size iron aluminate particles are mainly present on the periphery of the iron.

SEM micrographs for the specimen 5AFe1100(2) worn out at 2.0 Kg load at different magnifications are shown in Fig. 6.8. The micrograph viewed at 200X (Fig. 6.8(a)) reveals the formation of highly dense homogenous composite system. Fig. 6.8(b) shows the SEM micrograph at 5000X which shows the erosion marks being made by the harder alumina particles. Fig. 6.8(c) exhibits the SEM micrograph of the specimen at 10000X.The overall morphology of the system in this microstructure shows the formation of nano size iron aluminate which is formed during reactive sintering of iron and alumina particles.

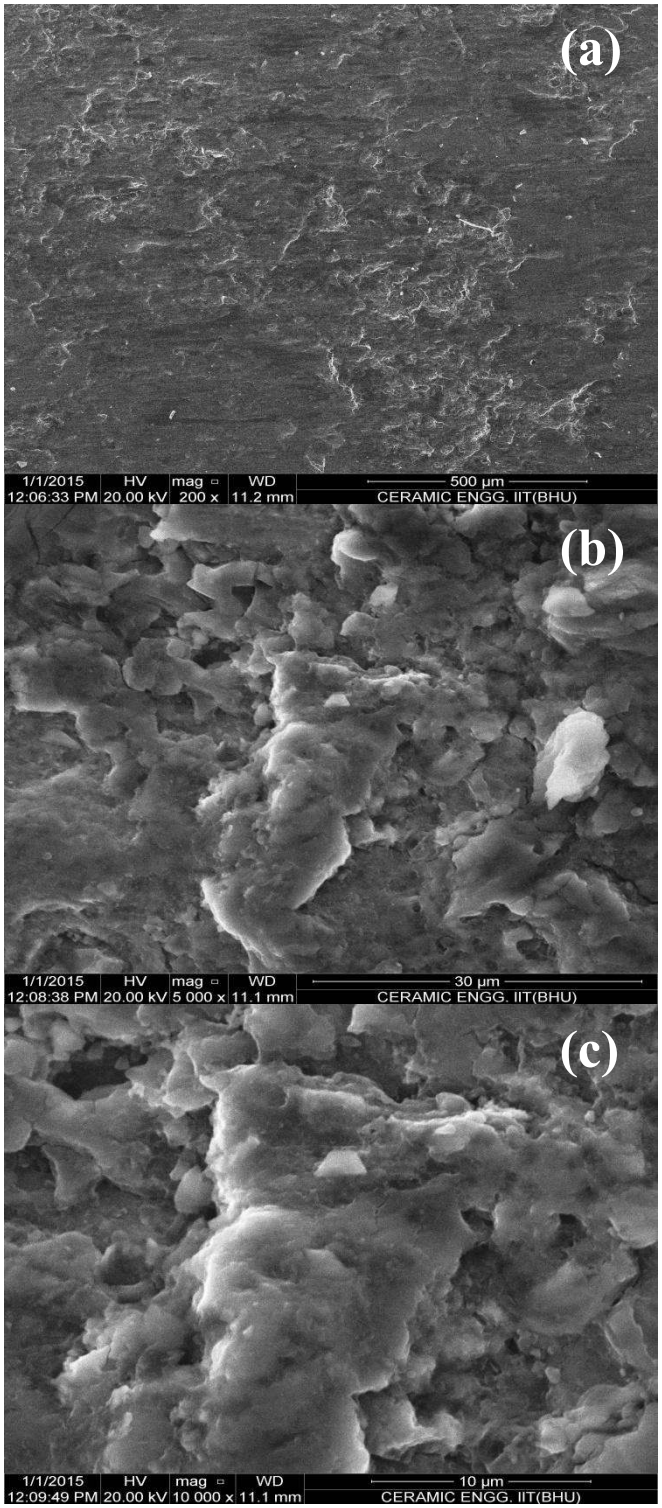

Fig. 6.6 SEM micrograph of 5AFe1000(3) (a) 200X (b) 5000X and (c)10000X magnification after measurement at 2 kg load

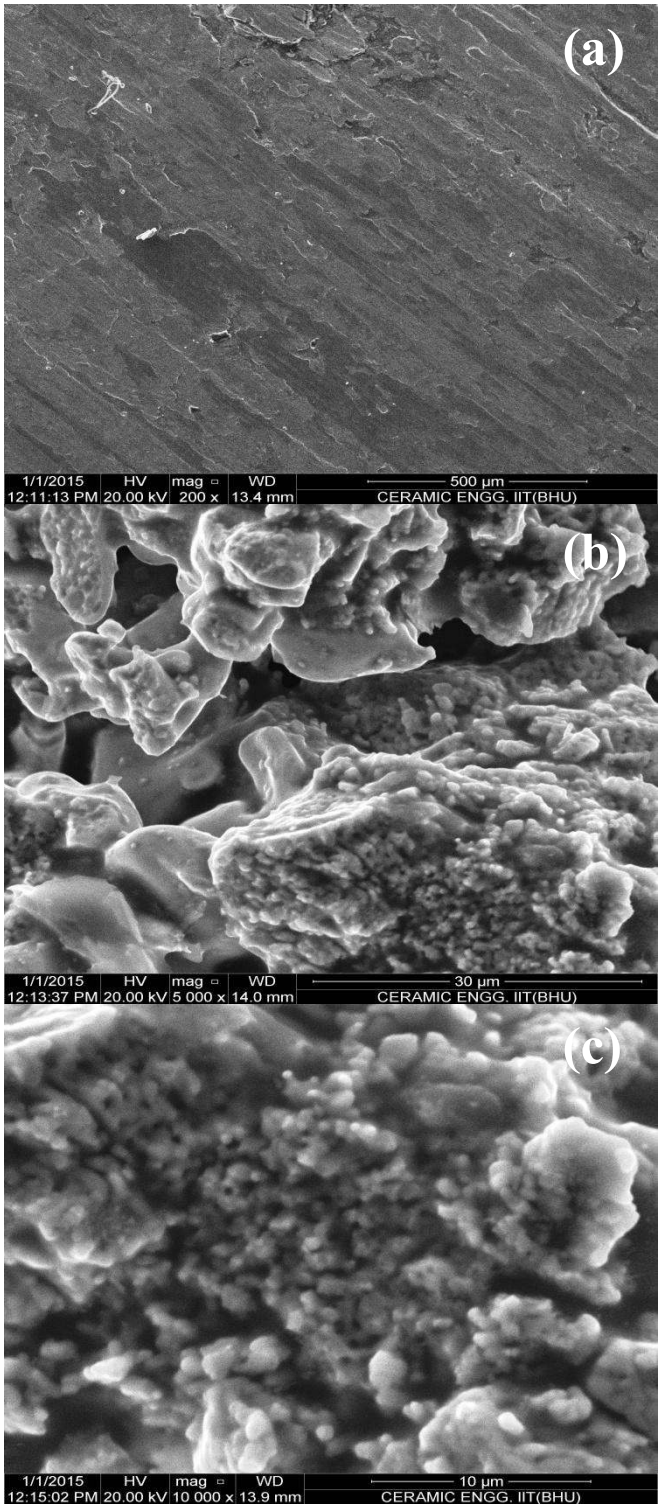

Fig. 6.7 SEM micrograph of 5AFe1100(1) (a) 200X (b) 5000X and (c)10000X magnification after measurement at 2 kg load

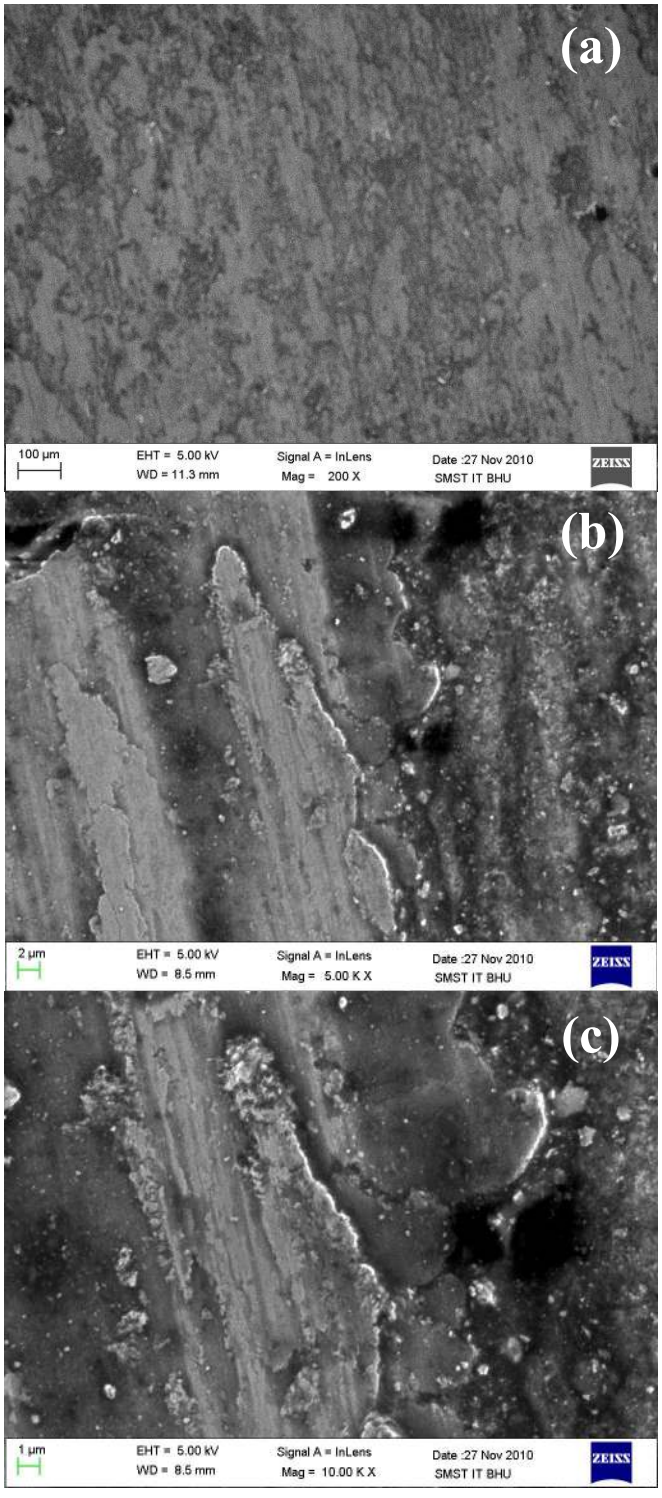

Fig. 6.8 SEM micrograph of 5AFe1100(2) (a) 200X (b) 5000X and (c) 10000X magnification after measurement at 2 kg load

In the present specimen, it was found that there was smoothening of the weared surfaces with the help of particles eroded from the specimen. Therefore, it was observed that in the present case the abrasive wear is more as compared to the adhesive wear. High magnification microstructures of specimens sintered at high temperature 1100°C i.e. Figs. 6.7 and 6.8 show greater bonding between grains. The particles coming out of the specimens add to wear of the surface due to abrasion contributing to smoothening or polishing effect.

Figs. 6.4, 6.5, 6.6 and 6.7 show the SEM micrographs of worn out surfaces of the specimens where the adhesive wear is prominent. Fig. 6.8 shows the SEM micrograph of worn out surface of the specimen where abrasive wear is prominent [Mazahery and Shabani (2012)]. It can be concluded from the above discussion that the wear rate of the specimens increases with an increase in the load. When the density and hardness values of the nanocomposite specimens are high, the wear rate of the nanocomposite specimens is low. Density and hardness of the specimen 5AFe900(1) are low due to low sintering temperature and time leading to small amount of wear at lower load i.e. 0.1290 mm^3/km at 0.5 kg load and wear rate (1.1406 mm^3/km) was high at a load of 2 kg (Fig. 6.1). At lower load, adhesive wear is prominent and at higher load abrasive wear is prominent. Formation of ceramic iron aluminate phase is also small in this specimen. The particle size of iron aluminate is in the range of 40-400 nm. With increase in sintering time, the densification and fraction of iron aluminate phase formed increases (5AFe900(2) – density 4.80 gm/cm^3; 5AFe900(3) – density 4.82 gm/cm^3). Their hardness increases leading to a lower wear rate. The wear rate increases with increase in load. However, the wear rate is lower than the specimen 5AFe900(1). The wear rate for 5AFe900(2) at 0.5 kg load was 0.0839 mm^3/km whereas it became 0.6427 mm^3/km under a load of 2.0 kg. The wear rate for the specimen 5AFe900(3) under 2 kg load is the lowest i.e. 0.5530 mm^3/km. For the specimens 5AFe1000(1), 5AFe1000(2) and 5AFe1000(3), there is only a marginal difference between the wear rate for all the loads ranging from 0.5 to 2.0 kg respectively. This is due to the fact that there is only a minute difference between the hardness numbers of these three specimens.

For specimen 5AFe1100(1), the density and hardness number are higher. Therefore, the wear rate values are lowest i.e. 0.1013 mm^3/km at 0.5 kg load and 0.4738 mm^3/km at 2 kg load. The wear rate values are also lower due to the optimum formation of iron aluminate ($FeAl_2O_4$) phase. When iron aluminate phase formation is much higher, appreciable amount of debris comes in between the disc and specimen surface which leads to the increased abrasive wear of the specimens. Therefore, with increasing sintering time, more aluminate phase forms leading to increased abrasive wear and specimens 5AFe1100(2) and 5AFe1100(3) have higher wear rate values under all loads. Wear rate for specimen 5AFe1100(2) is 0.1825 mm^3/km at a load of 0.5 kg and 0.6630 mm^3/km under a load of 2.0 kg. The wear rates for specimen 5AFe1100(3) are 0.0969 mm^3/km under0.5 kg and is 0.5759 mm^3/km under 2.0 kg.

The mechanism of wear in the present case can be explained as: at lower load i.e. at 0.5 kg, the adhesive wear is more prominent. When the two surfaces are clean and polished, the entire real area of the contact undergoes adhesion. In any of the situation where the adhesion occurs at the interface and tangential motion is imposed on the surfaces to cause one to move relative to the other, shear must take place to rupture the adhesive bonds at the interface to accomplish the tangential motion. In practice, the bonds rarely rupture at the interface; instead, the bonds of the cohesively weaker of the two materials rupture. The cohesively weaker material transfers to the cohesively stronger material. This results in adhesive wear or the loss of material from one surface as a result of the adhesion process. On the other hand, at high load i.e. at 2 kg, the wear is prominently abrasive. In practice there are two ways by which the abrasive wear can take place. In the first mode, the removed material i.e. debris is dragged tangentially across the surface, which will skive or cut a piece of material from the solid surface. When the surfaces are in dry sliding state, the material can be removed in the form of small nano/micron size particles from the specimens itself. In practical applications, it so happens that there are number of particles which act as cutting surfaces. Some have sharp edges that do cutting and others deform the material rather than cutting because they have become dull as a result of the grinding process.

A second mode or mechanism by which abrasive wear can occur is the situation where a high cohesive strength material like aluminum oxide in the present case may get trapped as individual particle between the two surfaces. This particle acts then as a cutting surface for removing material and thus produce scoring marks on the surface of the specimen. In these composite specimens, the amount of wear at high load is quite appreciable as compared to that at low load due to the entrapment of debris in between the two surfaces. The hard debris can produce abrasion of surfaces during the sliding contact and scoring marks are produced on the surface of the specimen (Fig. 6.5). Thus, second type of abrasive wear mechanism is prominent for different composite specimens at higher loads.

Overall wear behaviour of the composite specimens with applied load and processing parameters can be correlated with their densification and hardness (Chapter 5). The density of the specimen increased on increasing the sintering temperature and time. Iron aluminate phase formed during reactive sintering. Amount of iron aluminate phase also depends on sintering temperature and time. At lower sintering temperature and higher sintering time i.e. specimen 5AFe900(3) shows an optimum amount of iron aluminate phase whereas the same optimum quantity of iron aluminate phase forms at higher sintering temperature and lower sintering time i.e. for the specimen 5AFe1100(1) respectively. The quantity of iron aluminate phase is responsible for the overall variation in the hardness. There are basically two types of the wear mechanisms which occur in the present composite system i.e. adhesive and abrasive wear. When a load is applied, bonding between the two surfaces in contact is enhanced significantly. This situation is in particular true for both dry as well as for wet tribological system. It has been observed many times that even a thick film of lubricant cannot stop the contact between the two intermediate surfaces. At lower loads the adhesive wear is prominent and there is removal of the material from specimen surface in an uneven manner. With higher loads, the debris is crushed and harder ceramic reinforcement is entrapped between the specimen and the disc giving rise to abrasive wear. When abrasive wear dominates, the wear rate increases sharply. Such wear also smoothen the weared surface.

6.2 Wear Behavior of Fe-10% Al_2O_3 Metal Matrix Nanocomposites

Iron - alumina based metal matrix nanocomposite specimens with following details were prepared using P/M technology:

Composition: 90% Fe (electrolytic grade with 99.5% purity) and 10% Al_2O_3 (active; particle size of 70-230 mesh).
Compaction Load: 7 Tons
Sintering Temperature Range: 900, 1000 and 1100°C
Sintering Time Range: 1, 2 and 3 hour
Sintering Atmosphere: Argon
Specimen Size: 12 mm diameter and height 20 mm

6.2.1 Dry Sliding Wear Characterization

Fig. 6.9 and table 6.2 shows the wear rate vs. load plots and values of wear rate at different loads respectively for specimen sintered for 1h. Specimen 10AFe900(1) shows the wear rate value of 0.1718 mm^3/km at a load of 0.5 kg. On increasing the load to 1.0 and to 2.0 kg the wear rate values increases significantly to 0.1836 mm^3/km and to 0.5054 mm^3/km. For specimen 10AFe1000(1) at 0.5 kg load, the wear rate was found to be 0.1162 mm^3/km, 1.0 kg load shows the wear rate of 0.1519 mm^3/km, 2.0 kg load shows the wear rate of 0.8267 mm^3/km. Specimen 10AFe1100(1) shows the wear rate of 0.0820 mm^3/km at a load of 0.5 kg, same specimen shows a wear rate of 0.1105 mm^3/km at a load of 1.0 kg and 0.3020 mm^3/km at a load of 2.0 kg. The specimen sintered at low temperature showed high amount of wear whereas on increasing the sintering temperature, the wear rate decreased significantly.

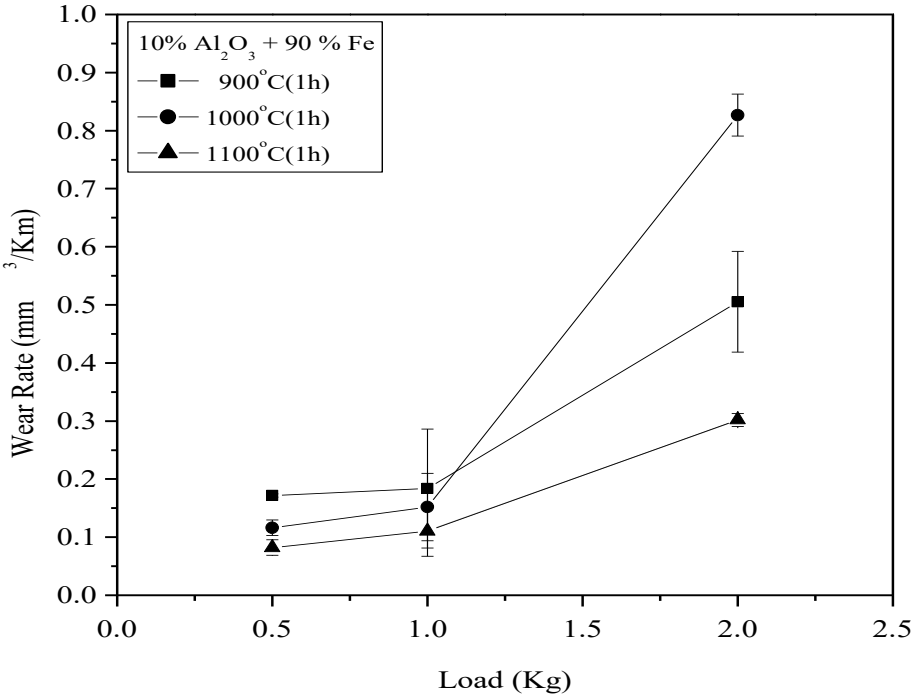

Fig. 6.9 Wear Rate vs. Load for specimens sintered for 1h

Table 6.2 Wear rate of different specimens at different loads for Fe-10% Al_2O_3 specimens

S. No.	Specimen Code	Wear Rate (mm^3/km) at 0.5 kg Load	Wear Rate (mm^3/km) at 1.0 kg Load	Wear Rate (mm^3/km) at 2.0 kg Load
1.	10AFe900(1)	0.1718	0.1836	0.5054
2.	10AFe900(2)	0.1359	0.2658	0.5504
3.	10AFe900(3)	0.0495	0.0997	0.4859
4.	10AFe1000(1)	0.1162	0.1519	0.8267
5.	10AFe1000(2)	0.0712	0.1988	0.5838
6.	10AFe1000(3)	0.0411	0.0871	0.3076
7.	10AFe1100(1)	0.0820	0.1105	0.3020
8.	10AFe1100(2)	0.0791	0.1891	0.5216
9.	10AFe1100(3)	0.1443	0.1543	0.3763

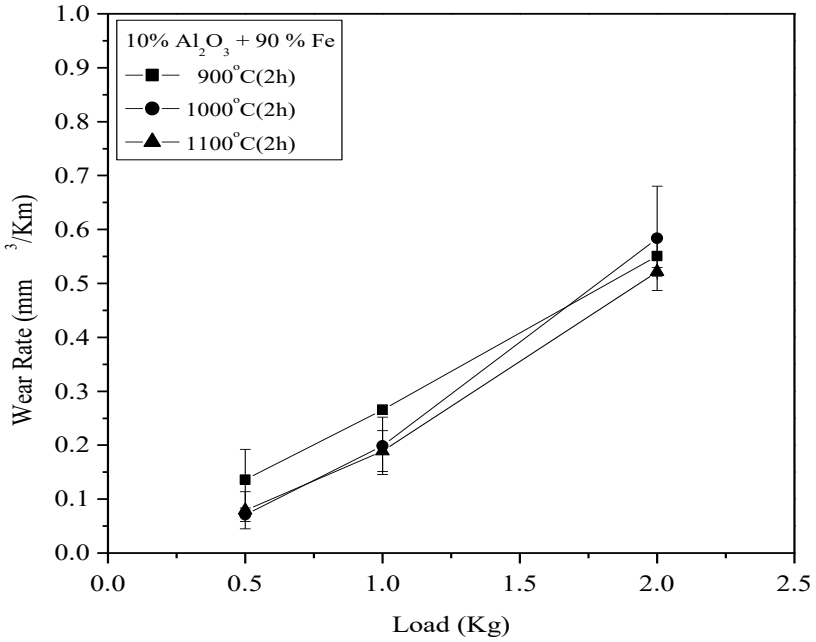

Fig. 6.10 Wear Rate vs. Load for specimens sintered for 2h

In a similar manner Fig. 6.10 and table 6.2 shows the wear rate vs. load plots and values of wear rate at different loads respectively for specimens sintered for 2h. The wear rate for the specimen 10AFe900(2) was found to be 0.1359 mm^3/km at 0.5 kg load; at 1.0 kg load the same specimen showed a wear rate value of 0.2658 mm^3/km and erstwhile at 2.0 kg load the wear rate of the specimen was found to be 0.5508 mm^3/km. Specimen 10AFe1000(2) showed a wear rate of 0.0712 mm^3/km at a load of 0.5 kg. Same specimen showed a wear rate of 0.1988 mm^3/km at a load of 1.0 kg; the wear rate of the specimen was found to be 0.5838 mm^3/km when tested at a load of 2.0 kg. On increasing the sintering temperature to 1100°C for 2 hour of sintering time the specimen 10AFe1100(2) showed a wear rate of 0.0791 mm^3/km at a load of 0.5 kg, the same specimen showed a wear rate of 0.1891 mm^3/km at a load of 1.0 kg, on increasing the load to 2.0 kg the specimen showed a wear rate of 0.5216 mm^3/km.

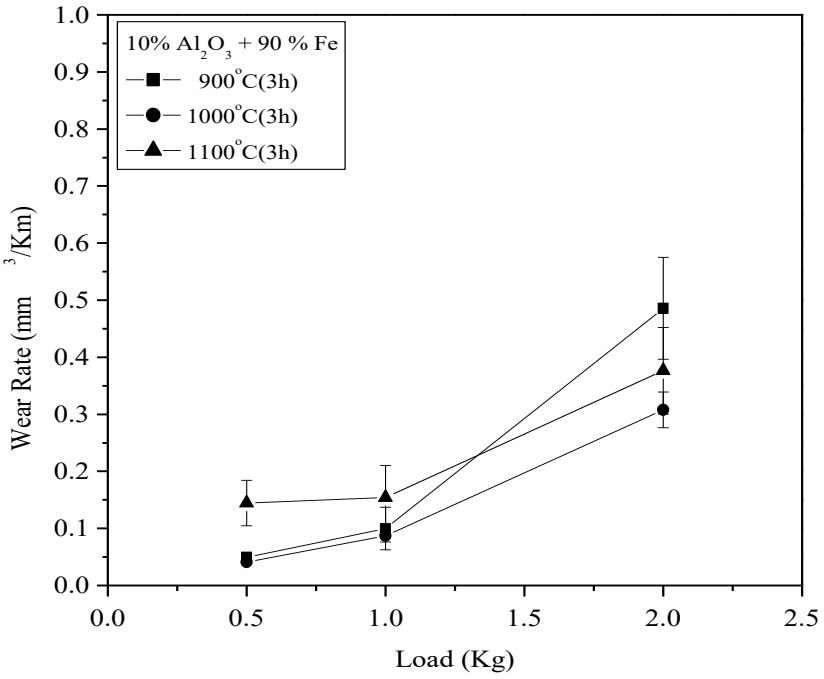

Fig. 6.11 Wear Rate vs. Load for specimens sintered for 3h

Fig. 6.11 and table 6.2 shows wear rate vs. load plots and values of wear rate at different loads respectively for specimens sintered for 3h. Specimen 10AFe900(3) shows a wear rate of 0.0495 mm^3/km at a load of 0.5 kg. On increasing load from 1.0 Kg to 2.0 Kg the wear rate values increased from 0.0997 mm^3/km to 0.4859 mm^3/km. For the specimen 10AFe1000(3) the wear rate at 0.5 kg load was found to be 0.0411 mm^3/km, at 1.0 kg load the wear rate was found to be 0.0871 mm^3/km and at 2.0 kg load the wear rate was found to be 0.3076 mm^3/km. On increasing the sintering temperature to 1100°C for 3 hours of sintering time, the specimen 10AFe1100(3) showed a wear rate of 0.1443 mm^3/km at a load of 0.5 kg. The same specimen showed a wear rate of 0.1543 mm^3/km at a load of 1.0 kg. On further increasing the load to 2.0 kg, the specimen showed a wear rate value of 0.3763 mm^3/km.

Fig. 6.12 and table 6.3 shows the Frictional force vs. load plots and values of friction force at different loads respectively for the specimens sintered for 1h.

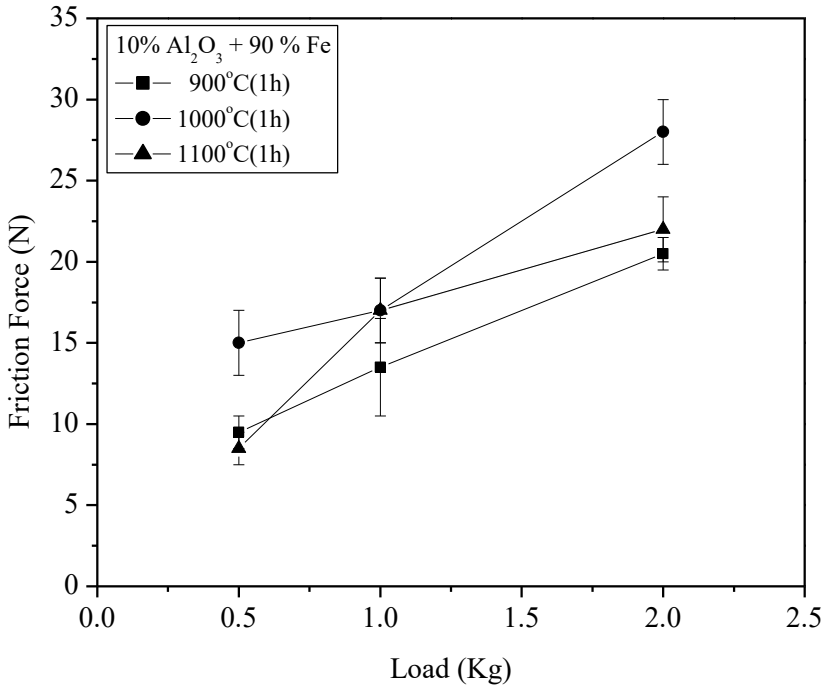

Fig. 6.12 Frictional Force vs. Load for specimens sintered for 1h

Table 6.3 Friction Force of different specimens at different loads for Fe-10% Al_2O_3 specimens

S. No.	Specimen Code	Friction Force (N) at 0.5 kg Load	Friction Force (N) at 1.0 kg Load	Friction Force (N) at 2.0 kg Load
1.	10AFe900(1)	9.5	13.5	20.5
2.	10AFe900(2)	8	14	20.5
3.	10AFe900(3)	6.5	13.5	18
4.	10AFe1000(1)	15	17	27
5.	10AFe1000(2)	13	20	22
6.	10AFe1000(3)	11	12	17
7.	10AFe1100(1)	13.5	27	22
8.	10AFe1100(2)	4.5	11	15
9.	10AFe1100(3)	3.5	11.5	16

Specimen 10AFe900(1) shows the friction force value of 9.5 N at 0.5 kg load, whereas the same specimen showed friction force value of 13.5 N at 1.0 kg load. On further increasing the load to 2.0 kg the same specimen showed friction force value of 20.5 N. The specimen which is sintered at 1000°C for 1 hour i.e. the specimen 10AFe1000(1) showed friction force value of 15 N, 17 N and 27 N at a load of 0.5, 1.0 and 2.0 kg respectively. On further increasing the sintering temperature to 1100°C and for 1 hour i.e. for specimen 10AFe1100(1) the friction force value was observed to be 13.5 N at 0.5 Kg load, 27 N at 1.0 kg load and 22 N at 2.0 kg load.

Fig. 6.13 and and table 6.3 shows the Frictional force vs. load plots and values of friction force at different loads respectively for specimens sintered for 2h. Specimen 10AFe900(2) shows the friction force value of 8.0 N at 0.5 kg load, whereas the same specimen showed friction force value of 14.0 N at 1.0 kg load. On further increasing the load to 2.0 kg the same specimen showed friction force value of 20.5 N. The specimen which is sintered at 1000°C for 2 hour i.e. specimen 10AFe1000(2) showed friction force value of 13 N, 20 N and 22 N at a load of 0.5, 1.0 and 2.0 kg respectively. On further increasing the sintering temperature to 1100°C and for 2 hour i.e. for specimen 10AFe1100(2) the friction force value was observed to be 4.5 N at 0.5 kg load, 11 N at 1.0 kg load and 15 N at 2.0 kg load.

In a similar manner Fig. 6.14 and table 6.3 shows the Frictional force vs. load plots and values of friction force at different loads respectively for specimens sintered for 3h. Specimen 10AFe900(3) shows the friction force value of 6.5 N at 0.5 kg load, whereas the same specimen showed friction force value of 13.5 N at 1.0 Kg load. On further increasing the load to 2.0 kg, the same specimen showed friction force value of 18.0 N. The specimen which is sintered at 1000°C for 3 hours i.e. specimen 10AFe1000(3) showed friction force value of 11 N, 12 N and 17 N at a load of 0.5, 1.0 and 2.0 kg respectively. On further increasing the sintering temperature to 1100°C and for 3 hours i.e. for the specimen 10AFe1100(3) the friction force value was observed to be 3.5 N at 0.5 kg load, 11.5 N at 1.0 kg load and 16 N at 2.0 kg load.

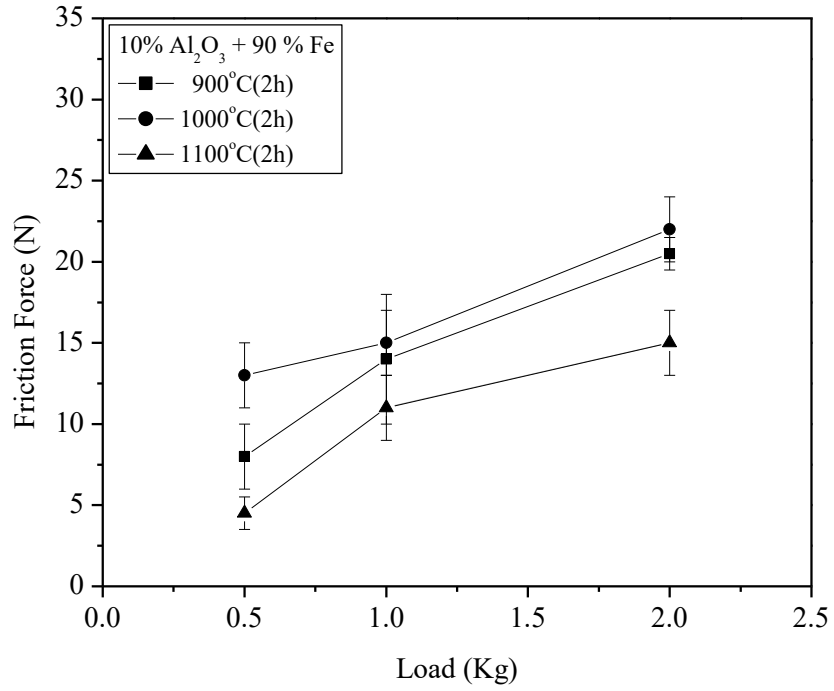

Fig. 6.13 Frictional Force vs. Load for specimens sintered for 2h

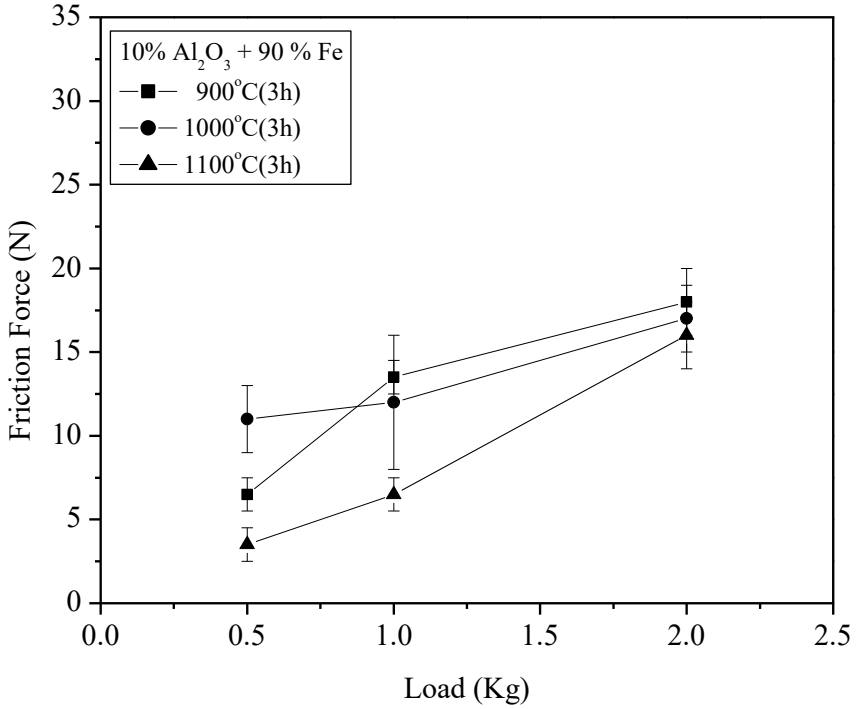

Fig. 6.14 Frictional Force vs. Load for specimens sintered for 3h

In some plots at some places intersection between the lines can be observed. These interactions in the plots could be related to the optimal iron aluminate phase formation. At these points, the wear rate values are found to be optimized with respect to the applied load. Beyond these points, the amount of the iron aluminate phase formation increases and thus at higher loads, the wear rate of the specimens increases. Due to this increase in the wear rate values, the wear mechanism was found to be abrasive (5% Al_2O_3) and micro ploughed (10% Al_2O_3) in nature which can be seen from the scanning electron micrograph of worn specimen.

6.2.2 Scanning Electron Micrographs of worn specimens

SEM of the worn out surfaces formed during the sliding wear were recorded in order to study the wear mechanism maps in the composite pins. Fig. 6.15 shows the SEM micrographs of the specimen 10AFe900(1) at (a) 200X (b) 500X and (c) 10000X magnification after 2.0 kg load. Micrograph of the specimen 10AFe900(1) at 200X magnification tested at 2.0 kg load is shown in Fig. 6.15(a). The microstructure shows the wear marks generated during the dry sliding contact between the steel disc and the composite pins. Initially the interaction of asperities on the disc and steel pin leads to the fragmentation and fracture at some asperities. The uneven removal of debris from the specimen surface indicates the sharp edges of the ceramic reinforcement particles which stand proud of the composite surface which may cut into the specimen surface and can generate the grooves. Even the test load on the specimen is 2.0 kg but still the amount of wear from the surface is not too much which in turn suggests the improved hardness of the composite pins. Fig 6.15(b) shows the micrograph of the specimen at 500X which depict removal of the material as well as the smoothing of the specimen surface. This smoothing takes place by the removal of the material which comes in between the disc and the specimen surface, thereby forming the tribofilm between the two. Fig. 6.15(c) shows the SEM micrograph of the specimen at 10000X which shows the formation of the nano size iron aluminate ($FeAl_2O_4$) phase along with some sub micron size particles of iron as well as aluminium oxide.

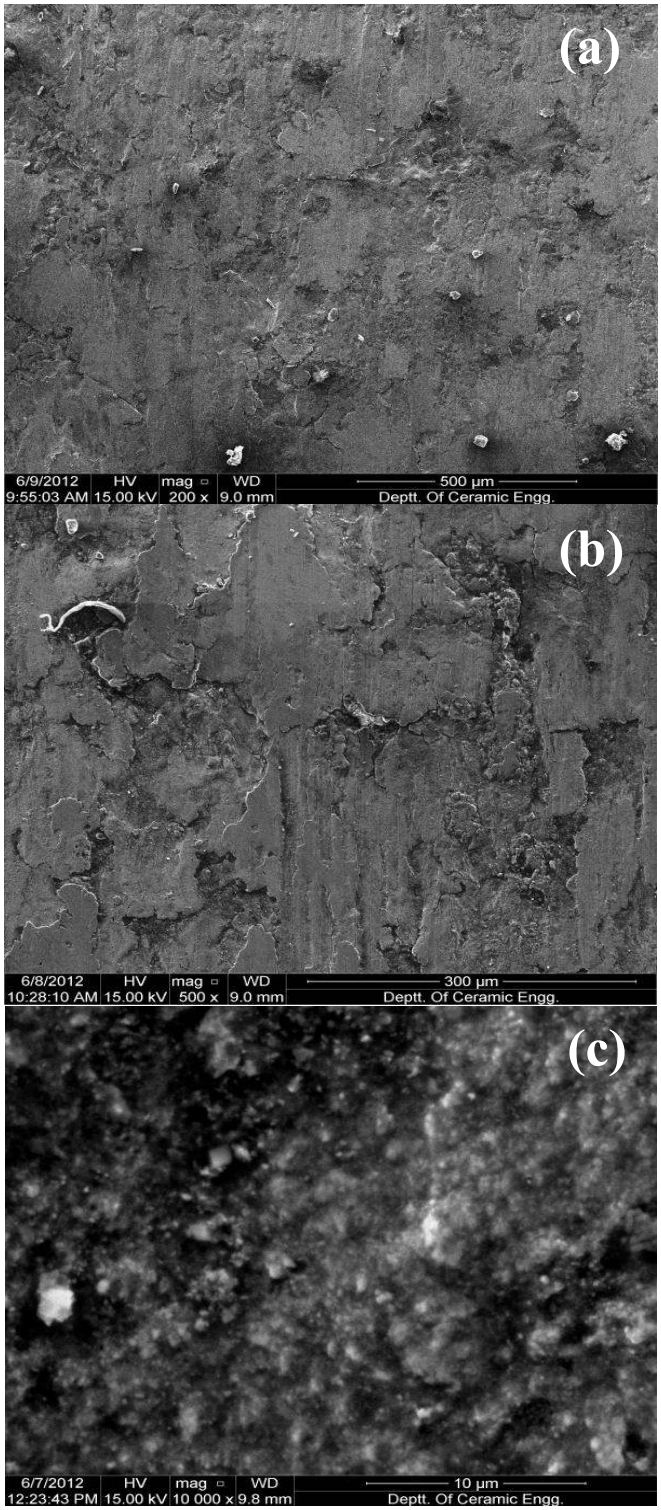

Fig. 6.15 SEM micrographs of specimen 10AFe900(1) at (a) 200X (b) 500X and (c) 10000X magnification after measurement at 2.0 kg load

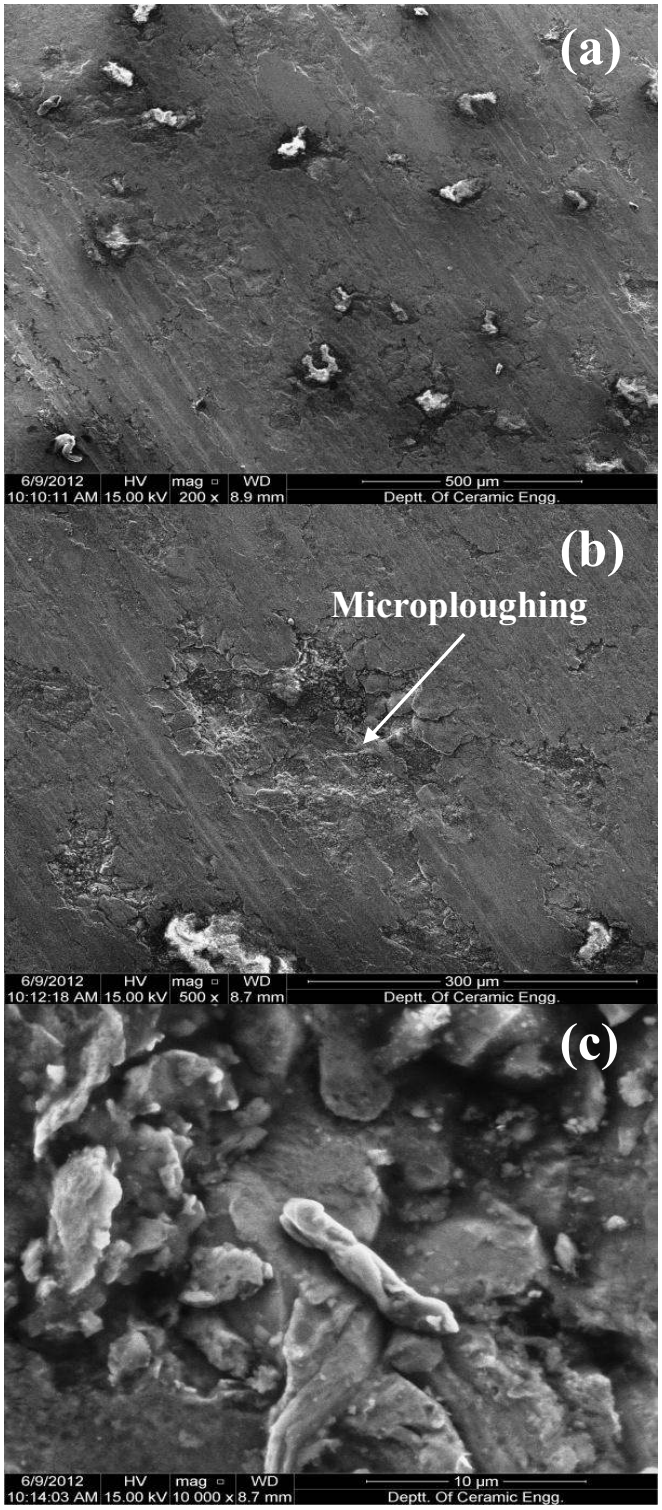

Fig. 6.16 SEM micrographs of specimen 10AFe900(2) at (a) 200X (b) 500X and (c) 10000X magnification after measurement at 2.0 kg load

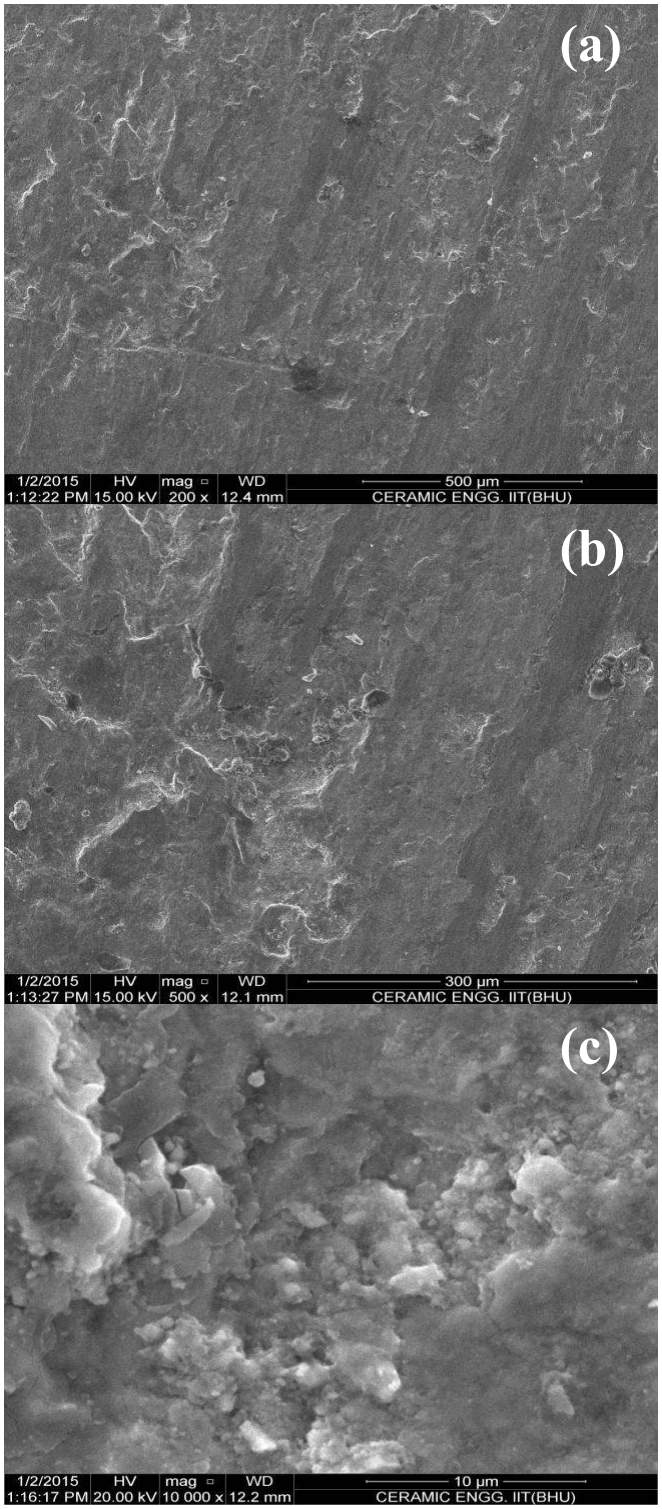

Fig. 6.17 SEM micrographs of specimen 10AFe900(3) at (a) 200X (b) 500X and (c) 10000X magnification after measurement at 2.0 kg load

Fig. 6.16 shows the SEM micrographs of the specimen 10AFe900(2) at (a) 200X (b) 500X and (c) 10000X magnification after 2.0 kg load. Fig 6.16(a) shows the micrograph at 200X magnification for specimen 10AFe900(2) worn out at 2.0 kg load. This micrograph shows the wear marks generated in a regular fashion and the generated grooves are more or less equal to the wear marks generated in the specimen 10AFe900(1). The micrograph also shows some grains of aluminium oxide being embedded in the iron matrix. Fig 6.16(b) shows the micrograph of the worn out specimen 10AFe900(2) at 500X, the wear in the present case takes place by the smoothing as well as by the microploughing effect on the specimen by the eroded particles. Fig. 6.16(c) shows the micrograph of the specimen 10AFe900(2) at 10000X which again reveals some sub micron size and some nano range particles of iron aluminate phase.

Fig. 6.17 shows the SEM micrographs of specimen 10AFe900(3) at (a) 200X (b) 500X and (c) 10000Xmagnification after measurement at 2.0 kg load. Fig. 6.17(a) shows the electron micrograph of the specimen at 200X illustrating the removal of the material by virtue of the adhesion effect. Due to higher sintering time, the overall removal of the material from the specimen surface is very low as can be seen from the generated wear marks. The adhesive effect in the present case is due to the plastic deformation of the particles. Fig. 6.17(b) shows the electron micrograph of the specimen at 500X illustrating the uniform removal of the material from the specimen surface. Due to the removal of the nano iron aluminate particles, some minute fretting effect can also be observed on the specimen surface. Fig. 6.17(c) shows the SEM image of the specimen at 10000X illustrating the presence of particles of iron, aluminium oxide and iron aluminate phase. Major amount of nano iron aluminate particles are present in the micrograph.

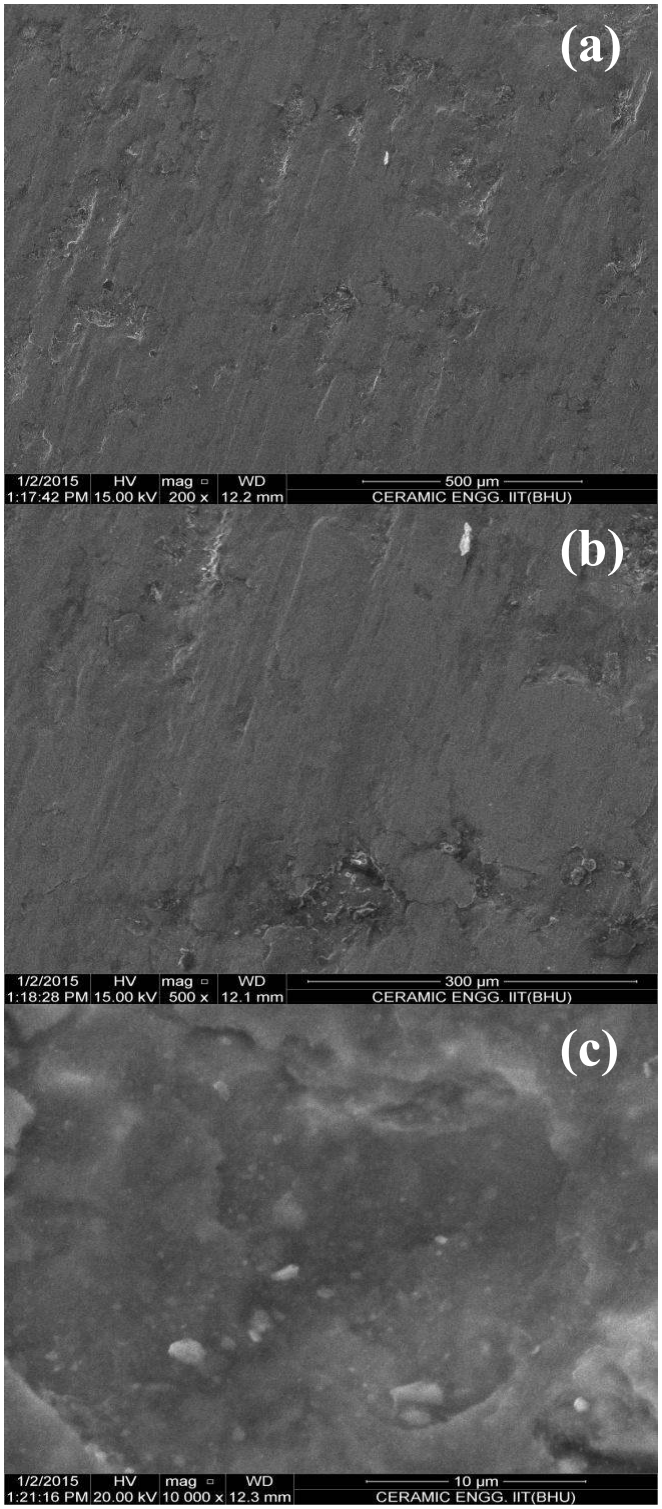

Fig. 6.18 SEM micrographs of specimen 10AFe1000(3) at (a) 200X (b) 500X and (c) 10000X magnification after measurement at 2.0 kg load

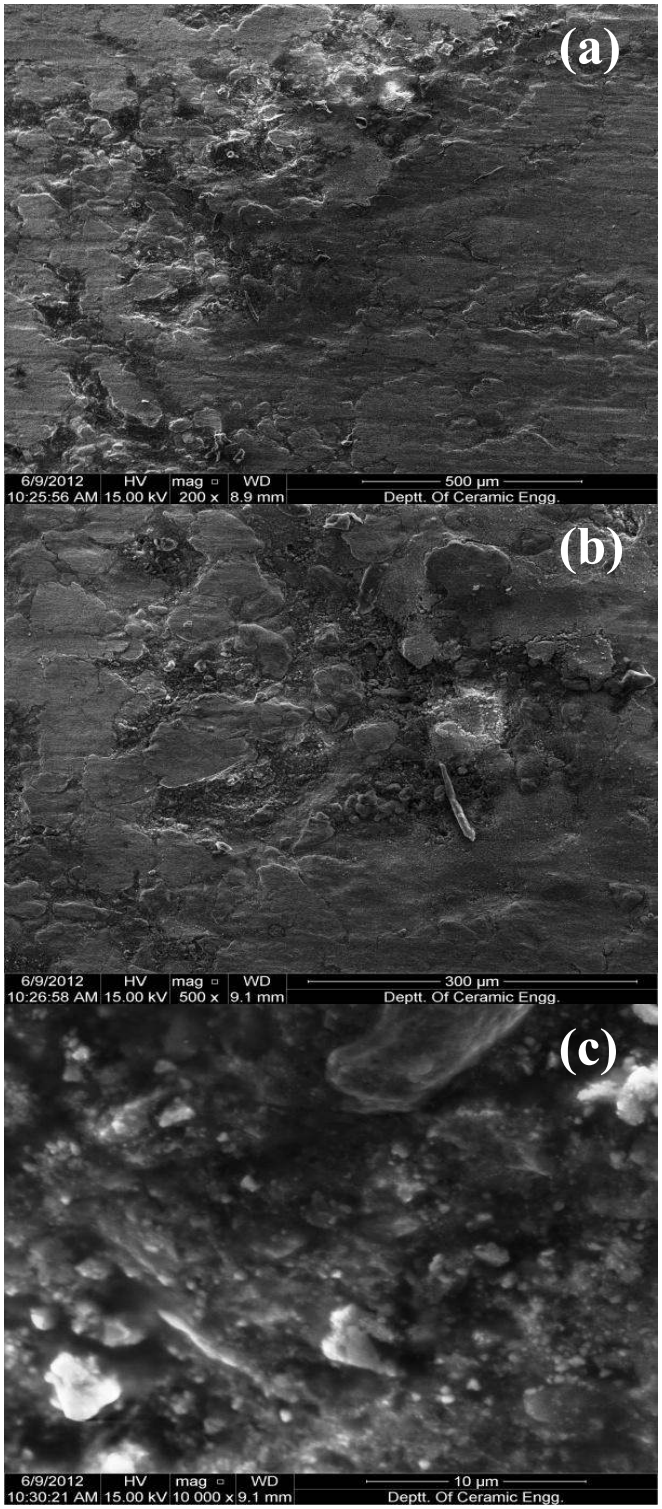

Fig. 6.19 SEM micrographs of specimen 10AFe1100(1) at (a) 200X (b) 500X and (c) 10000X magnification after measurement at 2.0 kg load

Fig. 6.18 shows the SEM micrographs of specimen 10AFe1000(3) at (a) 200X (b) 500X and (c) 10000X magnification after measurement at 2.0 kg load. Fig. 6.18(a) shows the electron micrograph of the specimen at 200X illustrating the removal of the material by virtue of the adhesion effect. Due to higher sintering time, the overall removal of the material from the specimen surface is very small as can be seen from the generated wear marks. The adhesive effect in the present case is also due to the plastic deformation of the particles. Fig. 6.18(b) shows the electron micrograph of the specimen at 500X illustrating the uniform removal of the material from the specimen surface. Due to the removal of the nano iron aluminate particles, some minute micro ploughing can also be observed on the specimen surface. Fig. 6.18(c) shows the SEM image of the specimen at 10000X illustrating the presence of particles of iron, aluminium oxide and iron aluminate phase respectively. Major amount of nano iron aluminate particles are present in the micrograph.

Fig. 6.19 shows the SEM micrographs of the specimen 10AFe1100(1) at (a) 200X (b) 500X and (c) 10000X magnification after wear at 2.0 kg load. Fig 6.19(a) shows the micrograph at 200X magnification for the specimen 10AFe1100(1) tested at 2.0 kg load. This shows the wear grooves and also intense wear marks generated due to the entrapment of the hard aluminium oxide particles between the disc and the specimen. In this micrograph a large concentration of material is removed from the specimen contact surface which has caused progressive wear by the action of the detached particles. This results in ploughing and the creation of surface grooves. Fig. 6.19(b) shows the micrograph of the specimen 10AFe1100(1) worn out at 2.0 kg load viewed at 500X, the specimen is abraded heavily by the hard ceramic reinforcement which is removed from the specimen surface thereby forming the tribofilm between the disc and the specimen itself. The same specimen when viewed at 10000X (Fig. 6.19(c)) revealed the formation of the iron aluminate phase with some micron and sub micron size particles of iron and aluminium oxide respectively. The presence of iron aluminate phase was also seen in the X-ray diffraction pattern of the representative composite specimen.

On the basis of the above discussion it can be concluded that at lower values of load i.e. at 0.5 kg, the wear from the pin is mainly due to fragmentation of asperities and removal of material is due to cutting and flowing action of penetrated hard asperities into the softer surface. Therefore, a higher amount of stress is expected to act on the asperities due to higher values of their hardness and sharpness. Because of this high value of stress levels at these points, the removed particles gets deformed plastically and some of the sharpest asperities gets fractured due to combined effect of normal and shear stress. It is also observed that in the initial period of wear mapping, a considerable amount of energy is spent on overcoming the frictional force which leads to heating of the contact surfaces. Thus, it is expected that initially the temperature of the contact surface is less and hence the asperities are expected to be more stronger and in more rigid form. As the time period increases, the wear from the pin is removed in a linear fashion and the temperature of the contact surface is also increased significantly. Due to the increase in the temperature of the contact surface, the asperities formed are mild and minute in nature.

At higher loads i.e. at 2.0 kg the initial wearing is similar to that of the wear which takes place at lower loads but as the time passess, the value of frictional heating increases which leads to higher temperature and softening of the surface materials. During sliding action, frictional force acts between the counter surfaces. This causes frictional heating between the disc and pin i.e. at the contact point. Since the two counter acting surfaces are in relative motion with respect to each other, the frictional heating is continuous because of insufficient time for heat dissipation. Initially, the asperities are stronger and sharper due to which the frictional force and as a result the frictional heating takes place at higher rate. After a certain period of time, because of the increase in flowability of the material on the specimen surface, slipping action is more which leads to the reduction of frictional heating. A higher possibility of adhesion between the counter surfaces leads to higher degree of friction. Because of these counter acting phenomena, frictional heating remains almost constant as observed.

The values of wear rate in all the specimen increases with an increase in the applied load values. The increase in the applied load leads to increase in the penetration of hard asperities of the counter surface to the pin surface. Beyond the critical load for each composite, the wear rate starts increasing abruptly with the applied load. The load at which wear rate increases suddenly to a very high value is termed as the transition load i.e. at 2 kg load. When the applied load is greater than the transition load, the wear rate of the composite shoots up to significantly higher value. This is attributed to the significantly higher frictional heating and thus the localized adhesion of the pin surface with the counter surface and also increase in softening of the surface material and thus more penetration of the asperities. Under such conditions, the material removal due to the delamination of adhered areas, microploughing, micro cutting and micro fracturing increases significantly. The overall variation of the wear rate and frictional force values were quite low and were found to depend on the iron aluminate phase formation which in turn depends on the sintering temperature and time respectively.

6.3 Deformation Behavior of Fe-Al_2O_3 Metal Matrix Nanocomposites

On the basis of the investigation regarding the sintering and hardness characterization of Fe-Al_2O_3 nanocomposites with variation of Al_2O_3 from 5% to 30% in iron matrix and processing parameters, it was found that optimum properties can be developed by suitable content of alumina and processing parameters. It was found that nanocomposites with 5% Al_2O_3 specimens sintered at 1100°C for 1h also show optimum mechanical behavior. Therefore, in order to study and understand the deformation behavior, 9 more specimens with 5wt% Al_2O_3 reinforcement were synthesized by sintering at 1100°C for 1h. The aim of this investigation was to differentiate the deformation behavior of nanocomposite specimens with different h/d ratios and interfacial frictional conditions. Therefore, after sintering, the specimens were machined on gap or extension type lathe machine to achieve the height to diameter (h/d) ratio of less than 1, equal to 1 and greater than 1. Specimens with h/d<1 had height, 9 mm and diameter, 15.2 mm (h/d=0.59). Specimens having h/d=1

had height, 12.8 mm and diameter, 12.8 mm (h/d=1.00). Specimens having h/d>1 had height, 16 mm and diameter, 11.3 mm (h/d=1.42). Density, hardness and microstructures of the specimens before and after the deformation were also recorded in order to get a deeper understanding of the deformation mechanism.

Deformation mechanisms refer to the various mechanisms at the grain scale that are responsible for accommodating large plastic strains in the composite material. The deformation mechanism in a material depends on the sintering temperature, deformation load, stress, grain size, presence or absence of an interfacial frictional condition and presence or absence of impurities in the material. Depending upon the deforming condition, some recrystallization may also occur in the grain as well as between the grain boundaries which leads to a fine grain size at an early stage followed by diffusive mass transfer processes.

6.3.1 X-Ray diffraction

Fig. 6.20 shows the X-Ray diffraction pattern of these specimens. The peaks of the XRD pattern were matched with the JCPDS data files of iron and aluminium oxide compounds.

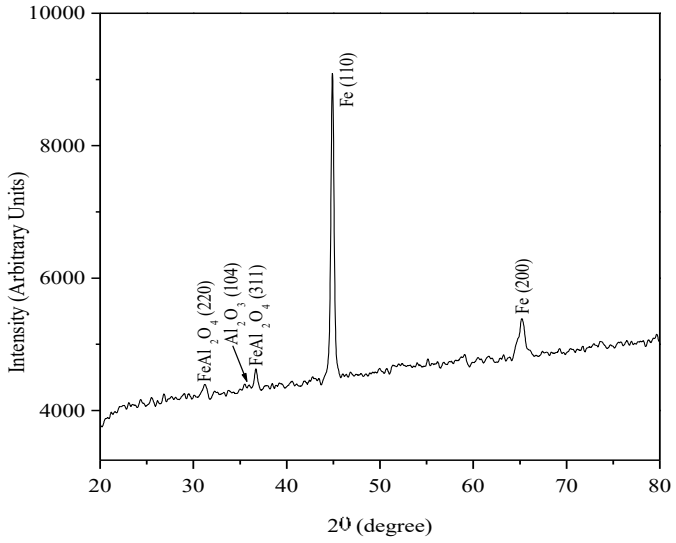

Fig. 6.20 X-Ray diffraction pattern of representative nanocomposite specimen

As reported earlier, it was found from the JCPDS files that the present composition contains iron (Fe), aluminium oxide (Al_2O_3) and iron aluminate ($FeAl_2O_4$) phases. The iron aluminate phase formation takes place due to reactive sintering between iron and alumina. All the XRD peaks were indexed.

6.3.2 Effect on Dimensional Changes

The deformation of the cylindrical Fe-Al_2O_3 nanocomposite specimens was carried out on a universal testing machine. The load on the specimens was increased gradually upto a safe load (4 Tons). After the deformation, the diameter and height of all the nanocomposite specimens was measured in order to determine the changes in their dimensions under different interfacial frictional conditions. A bulge profile was generated using AUTOCAD 2008 software. Fig. 6.21 (a) shows % Increase in specimen diameter for dry, solid lubricant and liquid lubricant conditions with different h/d ratios. It was found from the results that for h/d<1 in dry condition, the % increase in diameter was 6.31%, whereas in solid lubricating condition it was 5.00% and for the liquid lubricating condition it was 5.65%.

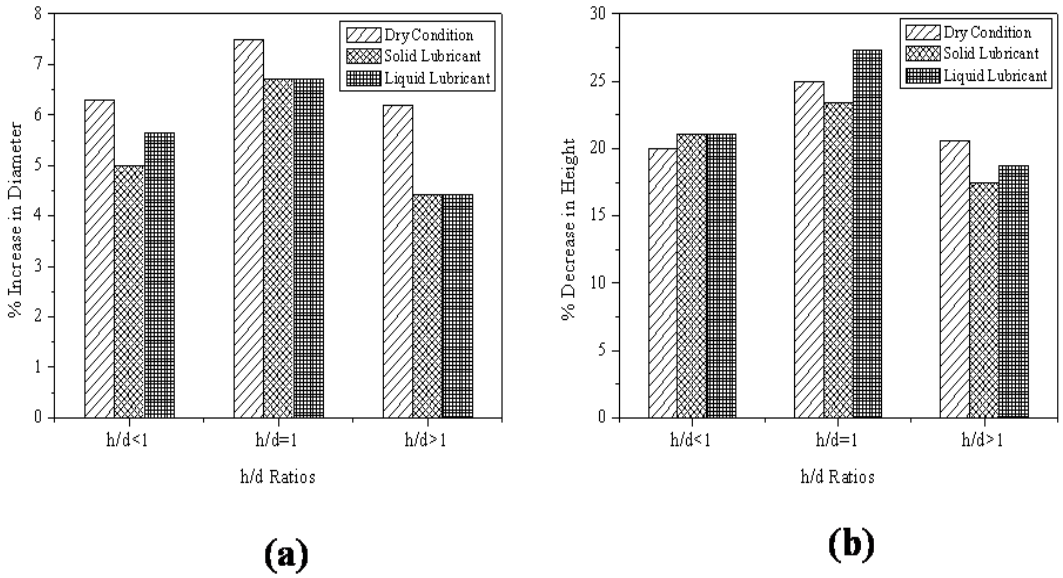

Fig. 6.21(a) % Increase in specimen diameter for dry, solid lubricant and liquid lubricant conditions with different h/d ratios (b) % decrease in specimen height for dry, solid lubricating and liquid lubricating conditions with different h/d ratios

For h/d=1, the values of % increase in diameter for the dry, solid and liquid lubricating conditions were found to be 7.50%, 6.71% and 6.71% respectively. Similar measurements for % increase in diameter were carried out for the h/d ratio greater than 1 (h/d>1) under dry, solid lubricant and liquid lubricant condition which showed the values 6.19%, 4.42% and 4.42% respectively. From the above investigations it was observed that for h/d<1, the highest percentage increase in diameter was for the specimen which was deformed in dry state, followed by the specimen whose deformation was conducted using liquid lubricant and being minimum for the specimen which was deformed using solid lubricant. Similarly, it can be seen that for h/d=1, the percentage increase in diameter value was highest for the specimen whose deformation was conducted in dry state whereas the values for the specimens lubricated with solid and liquid lubricant were same. However, for h/d>1 this increase was again highest for the specimen whose test was conducted in dry state and the values were same for the specimen whose test was conducted in solid and liquid lubricating conditions.

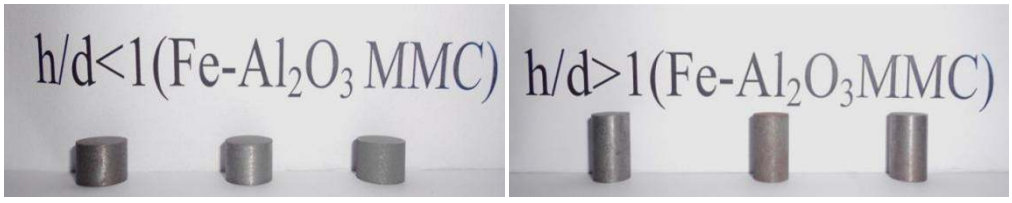

(a) **(b)**

Fig. 6.22 Undeformed Fe-Al_2O_3 nanocomposite specimens (a) h/d<1 and (b)h/d>1

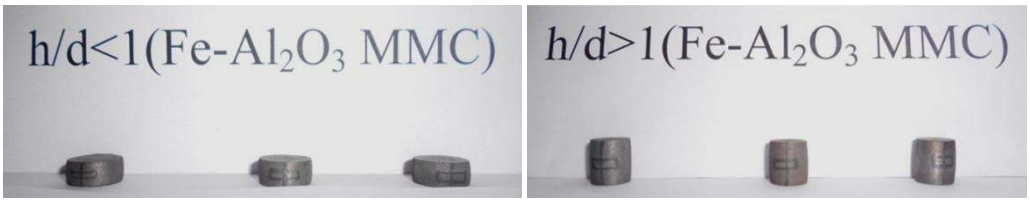

(a) **(b)**

Fig. 6.23 Deformed Fe-Al_2O_3 nanocomposite specimens tested under different interfacial conditions (a) h/d<1 and (b) h/d>1

Therefore, it can be concluded that the bulging was least in the specimen having h/d ratio greater than 1 and tested using solid and liquid lubricants. It can also be concluded that the bulging was maximum for the specimen having h/d=1 tested in dry condition.

Fig. 6.21(b) shows % decrease in the height for dry, solid lubricating and liquid lubricating conditions with h/d ratios. It can be seen from the results that for h/d<1 in dry condition the % decrease in height was found out to be 20.00% whereas for the solid lubricating condition it was found out to be 21.11% and for the liquid lubricating condition it was again found out to be 21.11%.

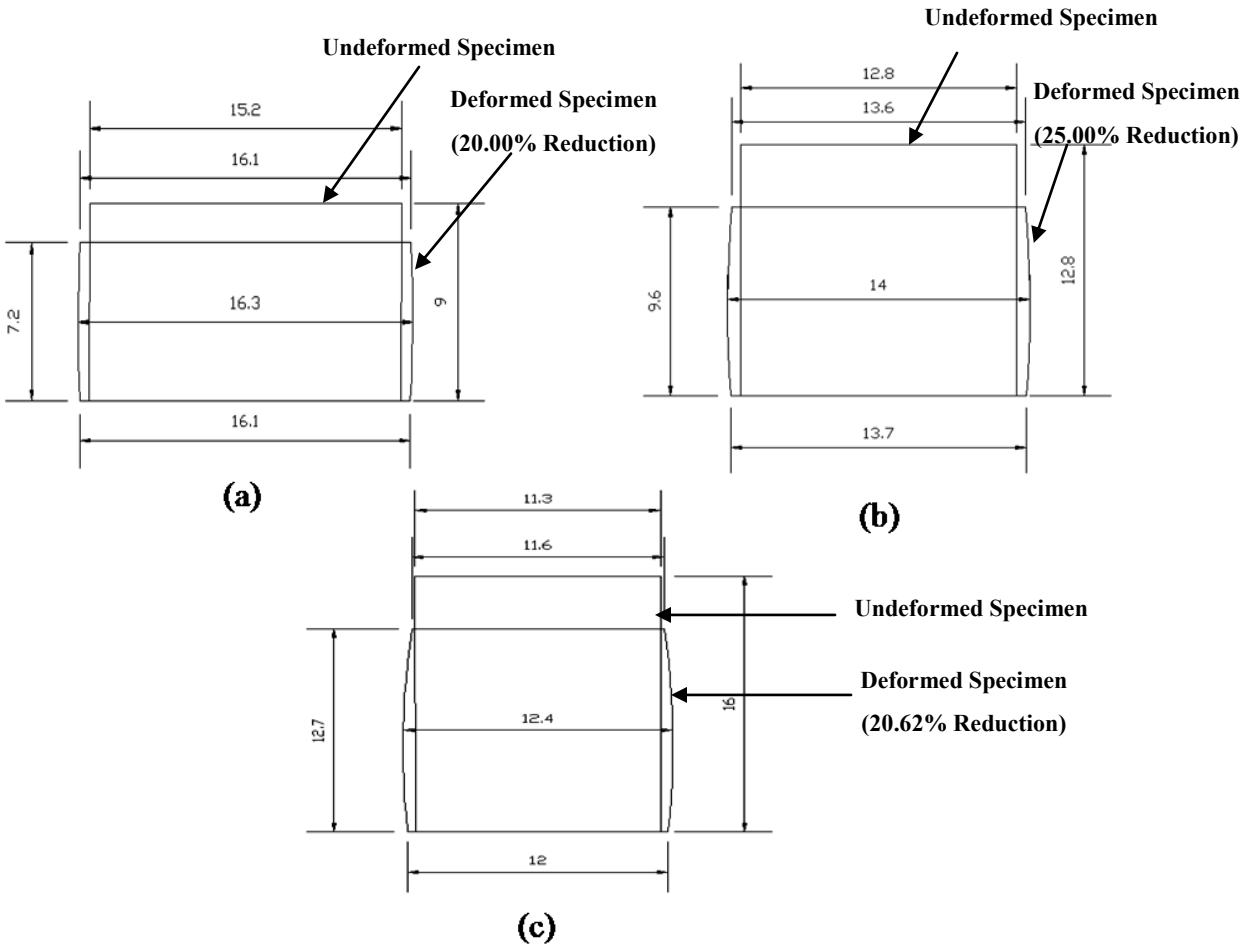

Fig. 6.24 Bulge Profile of the specimens having (a) h/d<1 (b) h/d=1 and (c) h/d>1 tested under dry condition (All dimensions are in mm)

Similarly for the specimens with h/d ratio equal to 1 (h/d=1) tested in dry, solid lubricating and liquid lubricating condition the % percentage decrease in height was found out to be 25.00%, 23.43% and 27.34% respectively. However, for the specimen with h/d>1 tested in dry, solid lubricant and liquid lubricant condition the % decrease in height were found out to be 20.62%, 17.50% and 18.75% respectively. It can be concluded from the above investigations that for h/d ratio less than 1 the highest % decrease in height was found for the specimen which were tested in solid and liquid lubricating condition and for dry condition it was found to be a little less than the previous two conditions. For the h/d ratio equal to 1, the decrease in height was highest for liquid lubricating condition, followed by dry condition and then solid lubricating condition.

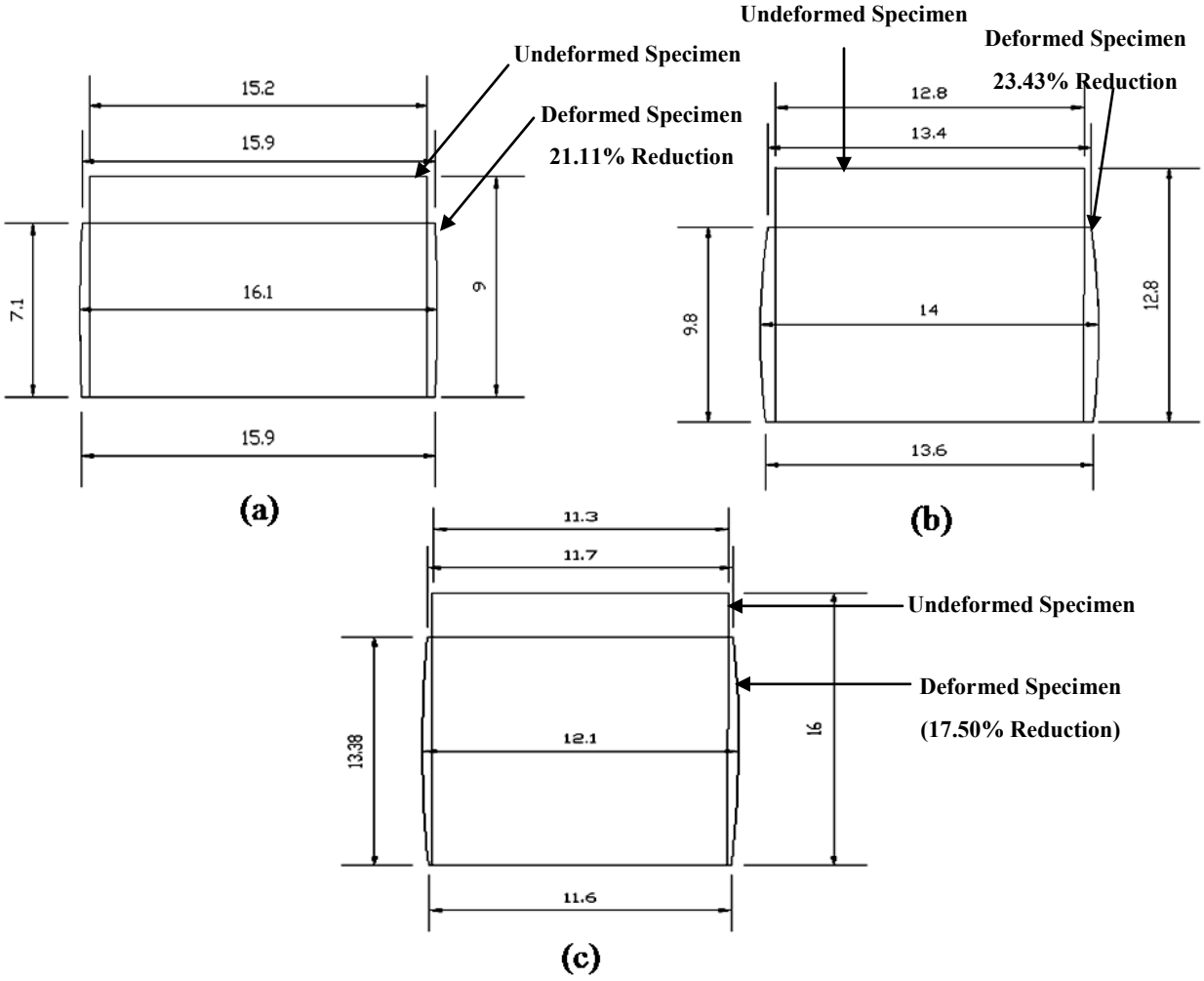

Fig. 6.25 Bulge Profile of the specimens having (a) h/d<1 (b) h/d=1 and (c) h/d>1 tested under solid lubricating condition (All dimensions are in mm)

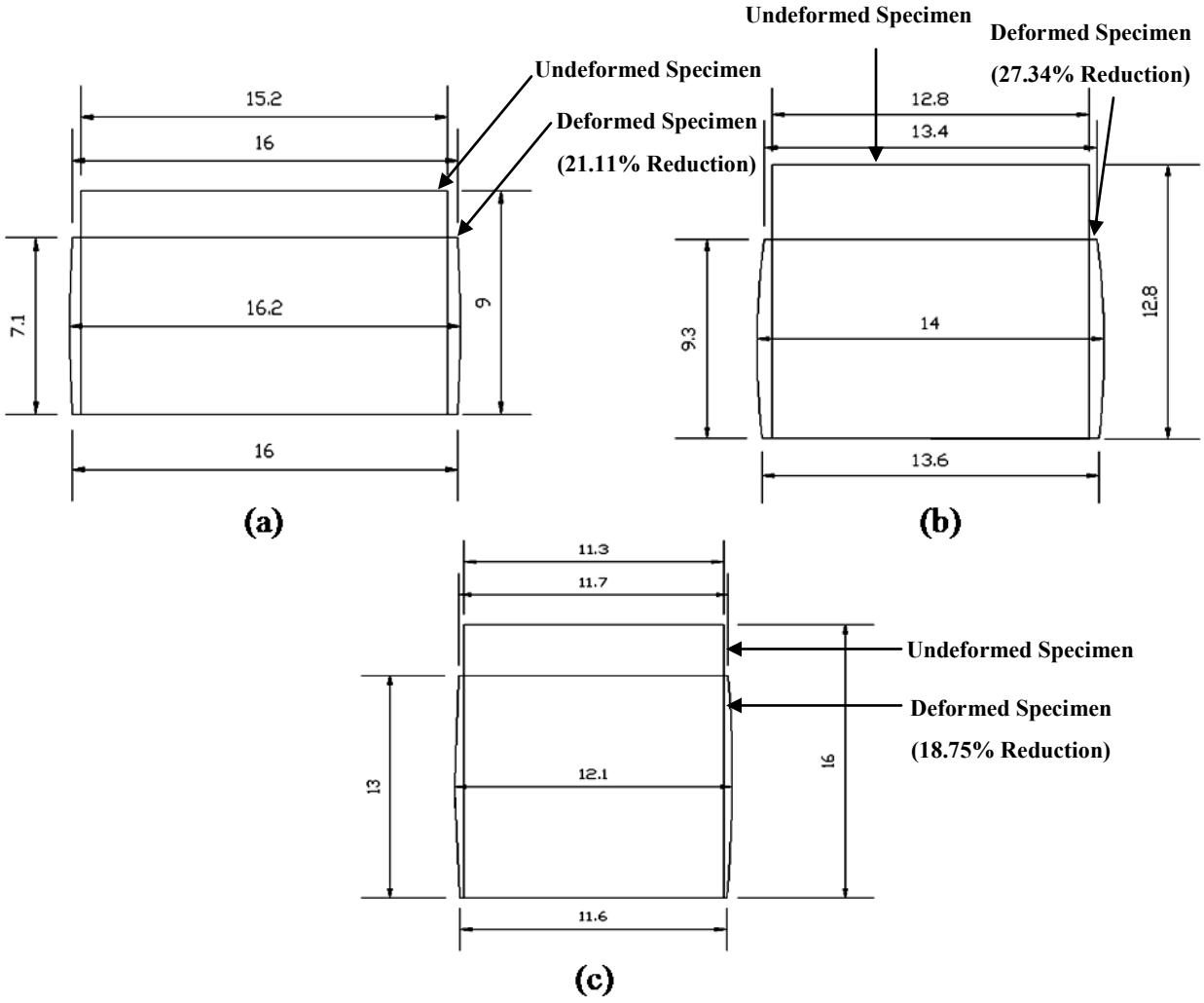

Fig. 6.26 Bulge Profile of the specimens having (a) h/d<1 (b) h/d=1 and (c) h/d>1 tested under liquid lubricating condition (All dimensions are in mm)

Finally for h/d ratio greater than 1 the % decrease in height was maximum for the specimen subjected to dry condition followed by liquid lubricating condition and then for solid lubricating condition. Therefore, it can be concluded that the % decrease in height value was lowest for the specimen having h/d ratio>1 and tested in solid lubricating conditions. The highest percentage decrease in height was found for the specimen having h/d=1 and tested in liquid lubricating condition. The specimen having h/d ratio greater than 1 and tested in solid lubricating condition gave the best optimum result i.e. having least % increase in diameter and % decrease in height values. % increase in diameter is less than % decrease in height leading to decrease in volume and increase in density as discussed in next sub-section.

Figs. 6.22 and 6.23 show the un-deformed and deformed Fe-Al_2O_3 nanocomposite specimens for h/d<1 and h/d>1 respectively. It can be observed from these two figures that there are no cracks present on the equatorial free surface of the specimen when tested under different interfacial conditions i.e. under dry, using solid lubricant and using liquid lubricant. Figs. 6.24, 6.25 and 6.26 show the bulge profile of the specimens having (a) h/d<1 (b) h/d=1 and (c) h/d>1 tested under different interfacial frictional conditions i.e. dry, solid lubricant and liquid lubricant respectively. The bulge profile of the deformed and undeformed specimen was drawn in AUTOCAD 2008 version. Mostly line tool with automatic input data was used in drawing all the bulge profiles. These bulge profiles help us to get a comparative idea of deformation characteristics of specimens of different shapes tested under different interfacial conditions.

6.3.3 Effect on Density and Porosity

Fig. 6.27 shows the difference of density of various specimens for green, sintered and deformed conditions. It was found from the diagram that for h/d<1 specimen tested in dry condition, the green density was 4.839 gm/cm^3, sintered density was 4.979 gm/cm^3 and deformed density was found out to be 7.227 gm/cm^3. For h/d ratio equal to 1 tested in dry condition yields specimen having green density as 4.800 gm/cm^3, sintered density as 4.9867 gm/cm^3 and deformed density as 6.878 gm/cm^3. Similarly the green, sintered and deformed density of the specimen having h/d ratio greater than 1 and tested in dry condition were found to be 4.807 gm/cm^3, 5.115 gm/cm^3 and 6.838 gm/cm^3 respectively. Moreover, the specimens tested with solid lubricant having h/d ratio less than 1 showed the green density 4.728 gm/cm^3, sintered density value as 5.011 gm/cm^3 and deformed density 7.045 gm/cm^3 respectively. With the same lubricant, specimens having height to diameter ratio equal to 1 showed green, sintered and deformed density as 4.750 gm/cm^3, 5.075 gm/cm^{3}and 6.950 gm/cm^3 respectively. Similarly the specimens having h/d ratio greater than 1 tested with solid lubricant showed green density as 4.763 gm/cm^3, sintered density as 5.003 gm/cm^3 and deformed density as 6.590 gm/cm^3.

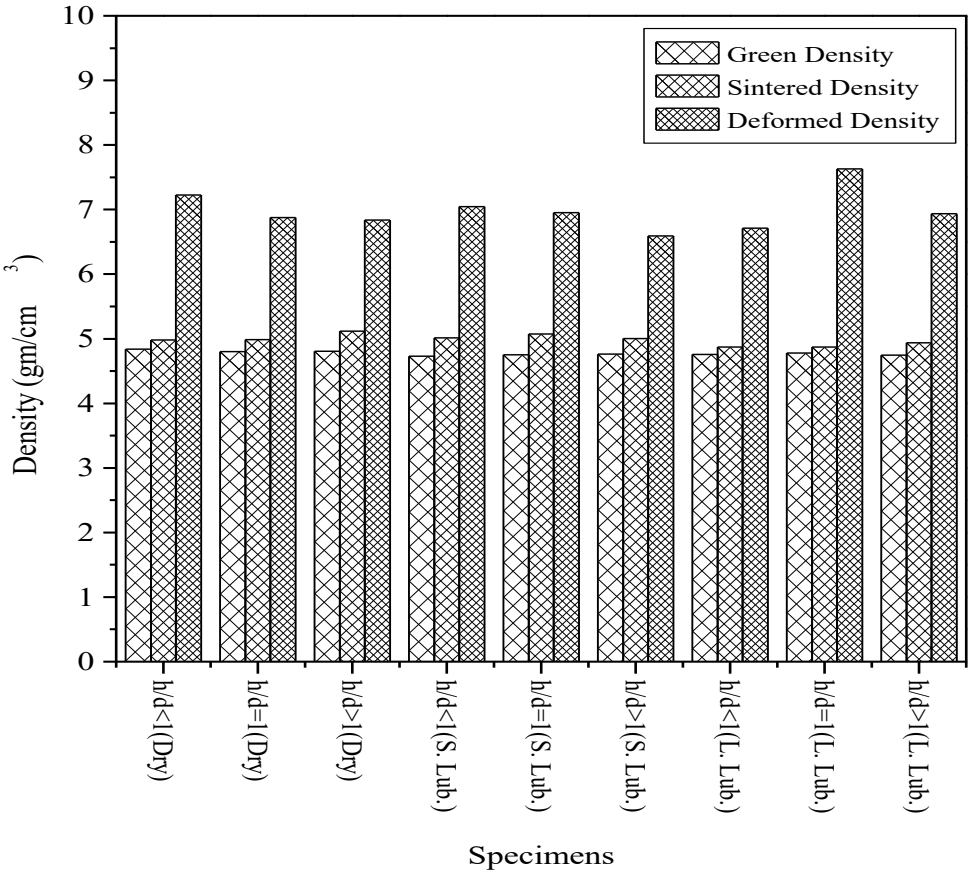

Fig. 6.27 Density vs. different h/d ratio specimens showing Green, Sintered and Deformed Conditions

Finally, for the specimens having h/d<1 tested with liquid lubricants show the green density 4.759 gm/cm^3, sintered density 4.870 gm/cm^3 and deformed density 6.710 gm/cm^3. Specimens having h/d=1 tested with liquid lubricant showed green density, sintered density and deformed density 4.777 gm/cm^3, 4.874 gm/cm^3 and 7.628 gm/cm^3 respectively. For the specimen having h/d >1 and tested with liquid lubricant showed, the value of green density as 4.745 gm/cm^3, sintered density as 4.940 gm/cm^3 and deformed density as 6.934 gm/cm^3.

Fig. 6.28 shows the % densification vs. h/d ratio for dry, solid lubricating and liquid lubricating conditions. For h/d ratio less than 1 the percentage densification value for

the specimen tested in dry condition was 45.14%, for solid lubricant was 40.59% and for liquid lubricant the value was 37.78%. Similarly, for height to diameter ratio equal to 1, percentage densification value for the specimen tested in dry condition showed a value of 37.92%, in solid lubrication it was found to be 36.95% and in the liquid lubrication condition it was found to be 36.11%. Finally, for h/d ratio greater than 1 tested in dry, solid lubricating and liquid lubricating condition showed % densification 33.67%, 31.71% and 40.37% respectively. From the above results, it can be concluded that the highest densification was for the specimen having h/d ratio less than 1 and tested in dry condition.

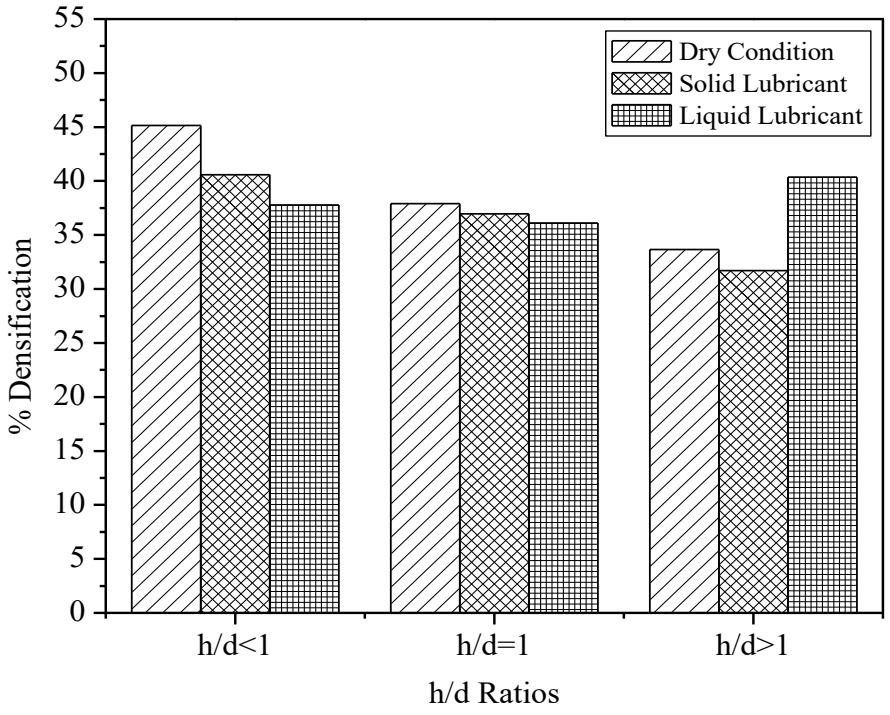

Fig. 6.28 % Densification vs. h/d Ratios for Dry, Solid Lubricating and Liquid Lubricating Conditions

It can be concluded from the above figure that the density of the sintered specimen are little higher than that of the green specimens and the deformed density of the deformed specimens is maximum. The reason for this change in density values can be understood as during the sintering process, there is binder removal and a little

consolidation of the powder particles due to which the voids or porosity removal is not high and density increases a little bit only. However, during deformation both types of processes i.e. grain deformation and grain boundary sliding occur which in turn help in the reduction of porosity. It results in significant increase in density of the specimens.

6.3.4 Effect on Hardness

Fig. 6.29 shows Hardness vs. h/d ratios before and after deformation for specimens tested under dry, solid lubricating and liquid lubricating conditions.

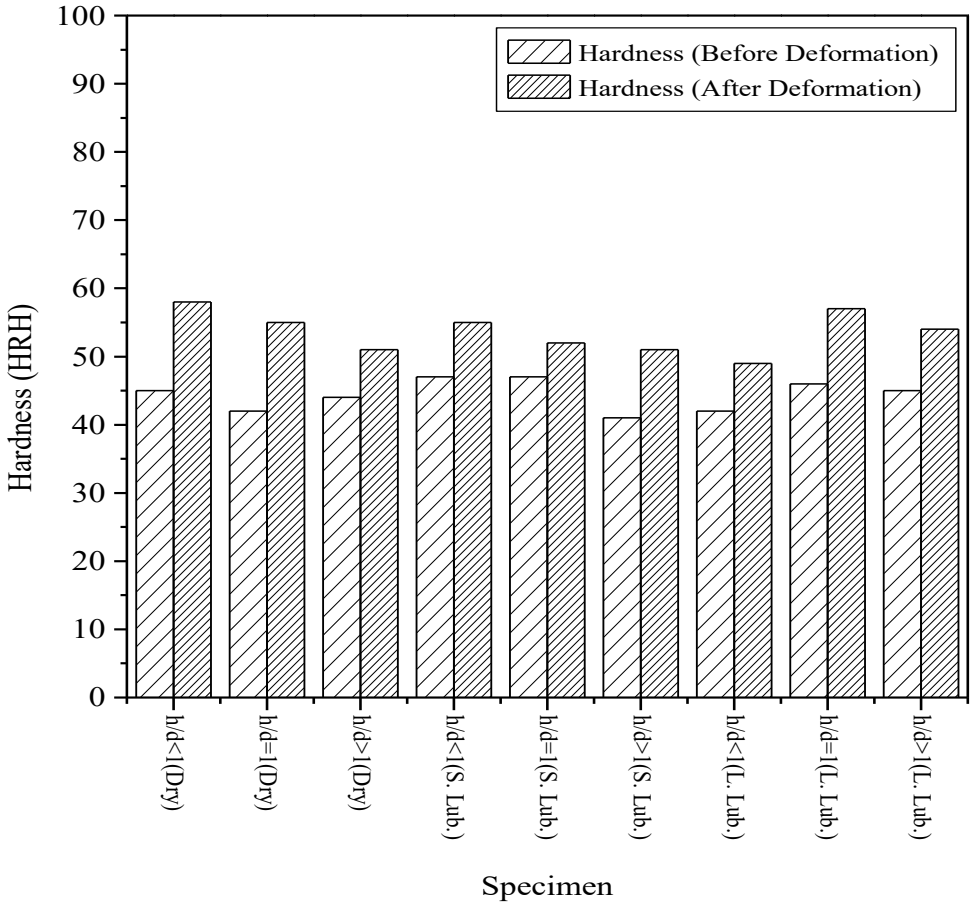

Fig. 6.29 Hardness vs. h/d Ratios for before and after deformation conditions

For h/d<1 tested in dry state, the hardness value before deformation was found to be 45 HRH and the hardness number after deformation was found to be 58 HRH. The specimen having h/d=1 and tested in dry condition has hardness number 42 HRH before deformation and it showed hardness number 55 HRH after deformation. The specimen having h/d ratio greater than 1 and tested under dry condition showed hardness number 44 HRH before deformation and 51 HRH after deformation.

The next spate of the specimens was tested with solid lubricant. In this, the specimen having h/d ratio less than 1 and tested under dry condition showed a hardness number 47 HRH before deformation and the same specimen after deformation showed the hardness number 55 HRH. The specimen having h/d=1 and tested with solid lubricant showed hardness number of 47 HRH before deformation and a hardness number 52 HRH after deformation. Similarly the specimen having h/d ratio greater than 1 tested with solid lubricant showed hardness number of 41 HRH before deformation and the same specimen showed hardness number 51 HRH after deformation.

The last slot of the specimens was tested with liquid lubricant. The specimen having h/d<1, tested with liquid lubrication showed the hardness number 42 HRH and the same specimen shows hardness number 49 HRH after deformation. Under the same lubricating condition, specimen having h/d value equal to 1 showed the hardness number 46 HRH and after deformation it shows hardness number 57 HRH. For specimens with h/d ratio greater than 1 using liquid lubricant hardness number before deformation was 45 HRH and it was 54 HRH after deformation. On the basis of the above discussion of hardness results, it can be concluded that the highest hardness number before deformation was found for the case having h/d ratio less than 1 and equal to 1 tested under solid lubricating condition. The highest hardness number after deformation was found for the specimen having h/d ratio less than 1 tested under dry condition. The increase in the hardness number of the deformed specimen was due to the grain interlocking and the reduction in the pore size.

6.3.5 Scanning Electron Microscopy

In order to study the effect of deformation on the grain, grain boundary and on the density the scanning electron micrographs of the specimens were recorded before deformation as well as after deformation.

(a) Before Deformation

In order to determine the morphology of the particles of the present composite system, scanning electron micrograph of the etched and unetched area of the polished surface of the nanocomposite specimen was recorded.

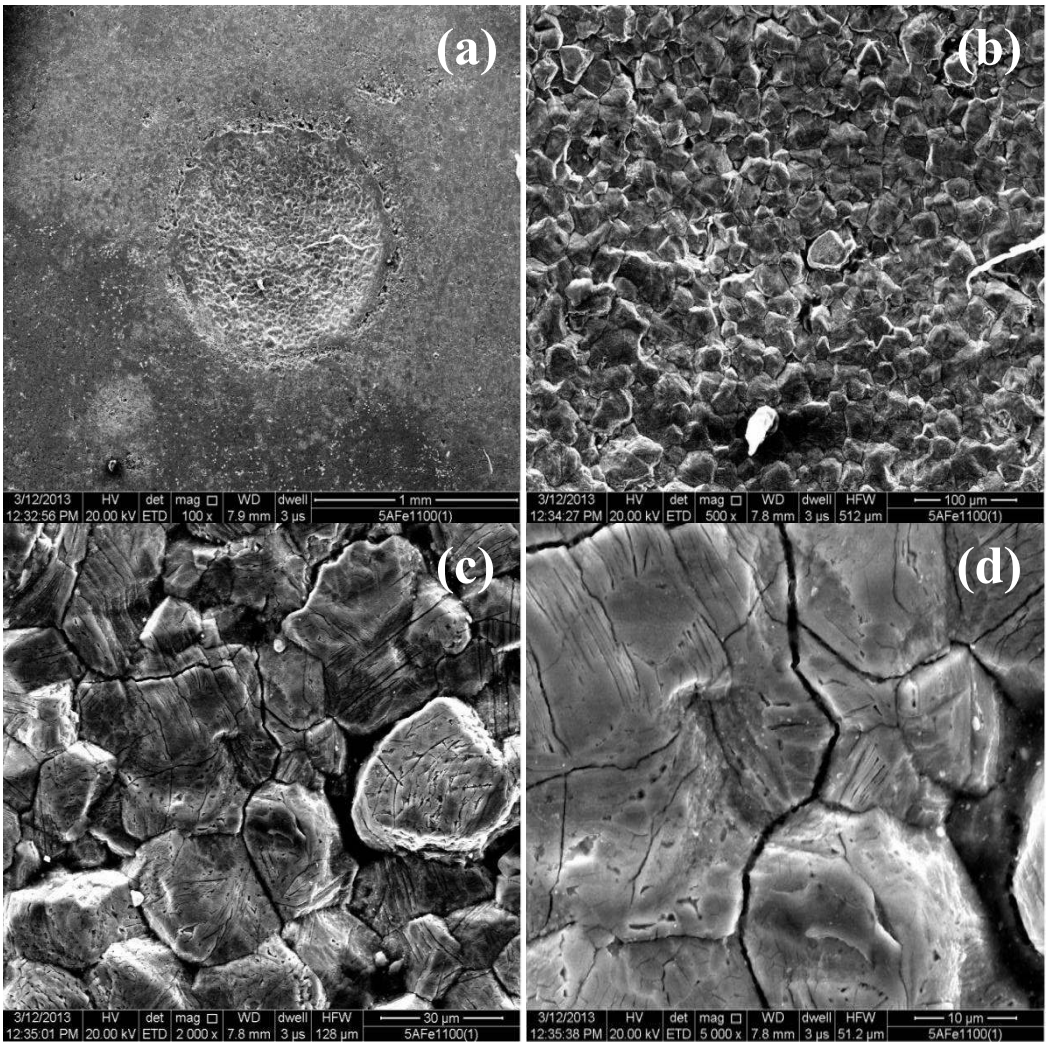

Fig. 6.30 Scanning Electron Micrograph of etched surface of specimen 5AFe1100(1) at (a) 100X (b) 500 X (c) 2000X and (d) 5000X magnifications

Fig. 6.30 shows the scanning electron micrograph of the etched surface of the specimen 5AFe1100(1) at (a) 100X (b) 500X (c) 2000X and (d) 5000X magnifications respectively. Fig. 6.30(a) shows the micrograph at 100X magnification which reveals the circular etched mark on the top surface of the specimen. Same specimen when viewed at 500X magnification [Fig. 6.30(b)] shows the highly dense phase composite structure having uniformly distributed grains of constituent phases. Similarly Fig. 6.30(c) shows the micrograph of the same specimen at 2000X which shows the strong bonding between the various grains with the presence of some sub micron size particles between the interstitial site of various grains. Fig. 6.30(d) shows the SEM of the present specimen at 5000X which shows the presence of some nano size particles in the bigger grain.

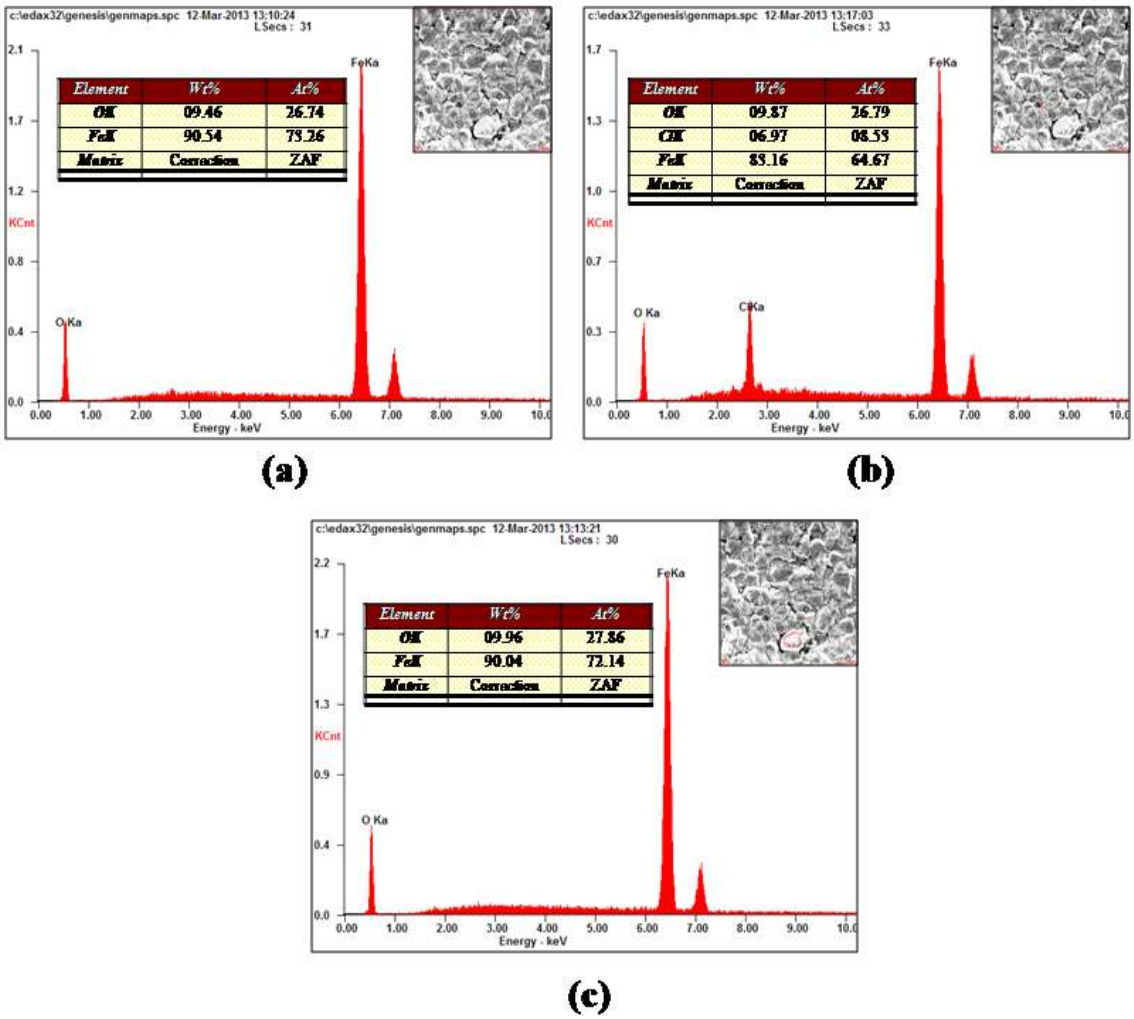

Fig. 6.31 EDAX and Compositional Analysis of the etched surface of the specimen 5AFe1100(1)(a) Full Frame (b) At a point and (c) On a particle

Fig. 6.31 shows the EDAX and compositional analysis of etched surface of the specimen 5AFe1100(1) (a) Full Frame (b) At a point and (c) On a particle. Fig. 6.31(a) shows the full frame EDAX of the specimen which shows the presence of iron (Fe) and oxygen (O_2). Oxygen is 09.46 wt% and iron is 90.54 wt%. Fig. 6.31(b) shows EDAX at a point which shows the presence of oxygen, chlorine and iron. Oxygen is 09.87 wt%, chlorine is 06.97 wt% and iron is 88.16 wt%. Fig. 6.31(c) illustrates the EDAX of a particle which again shows the presence of oxygen and iron. Oxygen is 09.96 wt% and iron is 90.04%. Due to use of HCl solution as the etchant, the ceramic phase has been eroded off and there is a presence of only Fe in the EDAX of the specimen.

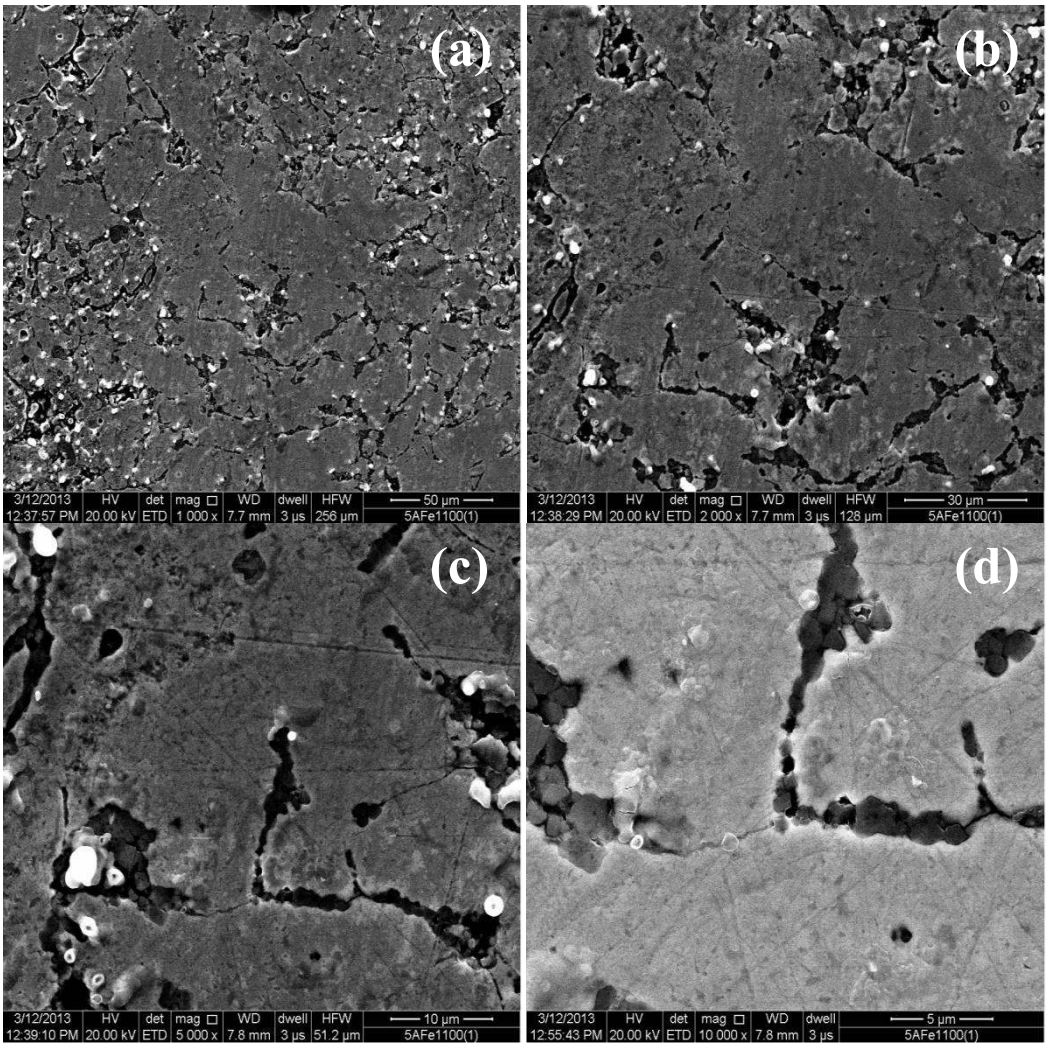

Fig. 6.32 Scanning Electron Micrograph of non-etched surface of specimen 5AFe1100(1) at (a) 1000X (b) 2000 X (c) 5000X and (d) 10000X magnifications respectively

Fig. 6.32 shows the Scanning Electron Micrograph of the non-etched surface of the specimen 5AFe1100(1) at (a) 1000X (b) 2000 X (c) 5000X and (d) 10000X magnifications respectively. Fig 6.32(a) shows the micrograph of the specimen at 1000X which shows a uniformly distributed dense phase composite structure with the presence of some nano size pores. Fig. 6.32(b) shows a higher magnification view of the same specimen at 2000X showing the presence of some micron size particles of Al_2O_3 along with some Fe particles lying mostly in the connected pore region of the composite structure. Fig. 6.32(c) and 6.32(d) shows the micrograph of the same specimen at 5000X and 10000X magnifications respectively which shows the black grains of iron (Fe), white grains of aluminum oxide (Al_2O_3) and greyish grains of iron aluminate ($FeAl_2O_4$) phase respectively. The grains of various constituent phases present are of size 1-2 μm along with some grains of nanometer size respectively.

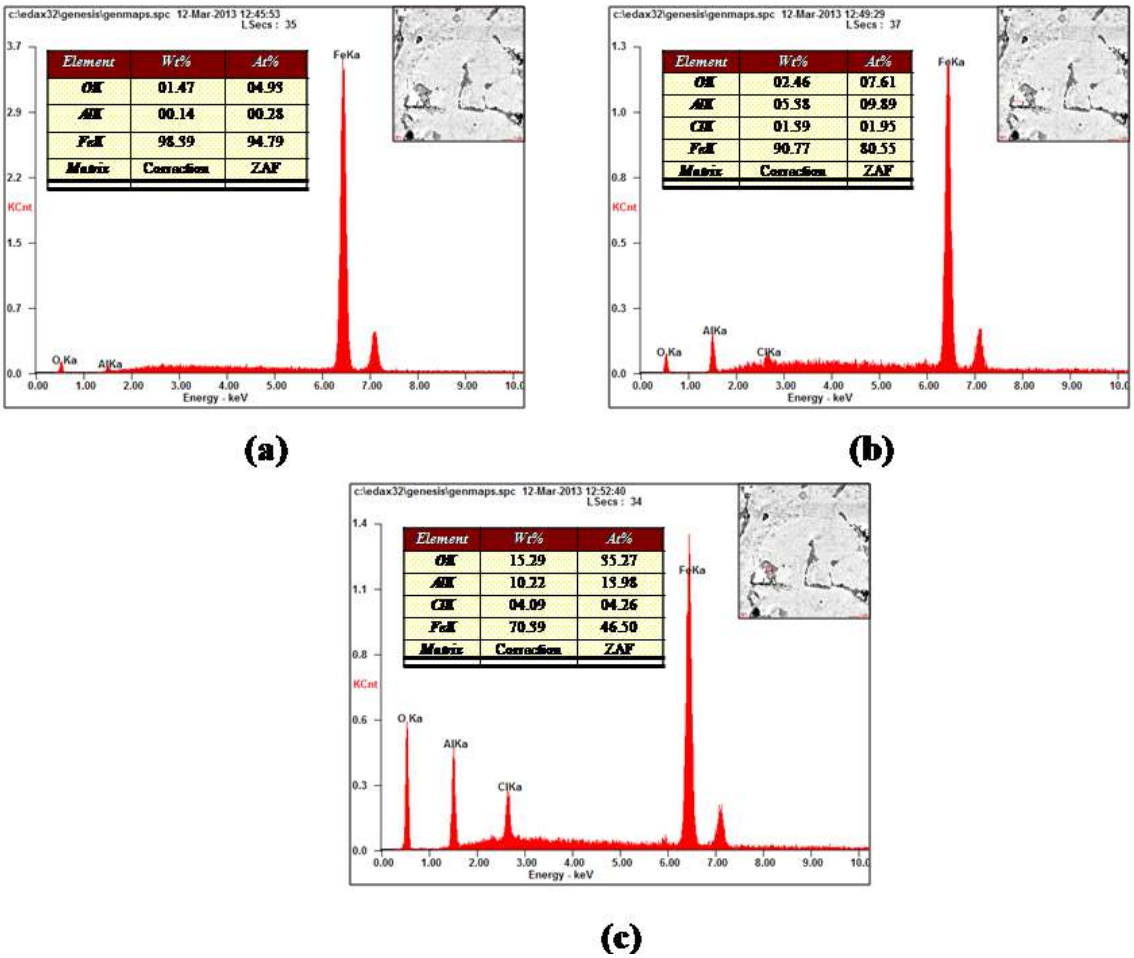

Fig. 6.33 EDAX and Compositional Analysis of non-etched surface of specimen 5AFe1100(1) (a) Full Frame (b) At a point and (c) On a particle

Fig. 6.33 shows the EDAX and compositional analysis of the non-etched surface of the specimen 5AFe1100(1) for (a) Full Frame (b) At a point and (c) On a particle. The full frame view [Fig. 6.33 (a)] shows the presence of mainly three elements namely oxygen, aluminium and iron respectively. The weight percentage of these three elements was found to be 01.47%, 00.14% and 98.89% respectively. Similarly, Fig. 6.33 (b) shows the EDAX results at a point which shows the presence of four elements namely oxygen, aluminium, chlorine and iron. Oxygen is 02.46 wt%, aluminium is 05.88wt%, chlorine is 01.89wt% and iron is 90.77wt%. Fig. 6.33 (c) shows the presence of same elements on a particle and the oxygen is 15.29 wt%, aluminium is 10.22wt%, chlorine is 04.09wt% and iron is 70.89wt%.

(b) After Deformation

Fig. 6.34 shows the SEM of deformed specimen with h/d<1 in dry state at (a) 100X (b) 500X (c) 2000 X (d) 5000X (e) 10000X and (f) 15000X. Fig. 6.34(a) shows the micrograph of the specimen at 100X magnification which shows a highly dense phase structure in comparison with the sintered condition. The same micrograph when viewed at 500X magnification (Fig. 6.34(b)) shows a considerable amount of reduction in the intragranular porosity. It also shows homogenously distributed grains of constituent phases. Fig. 6.34 (c) shows the SEM of the same specimen at 2000X magnification which indicates the entrapment of fine nano size iron aluminate particles in the intragranular pores of the specimen. Due to this filling of the nano particles in the pores of the specimen, the specimen achieves much more densification. The same specimen when viewed at 5000X magnification (Fig. 6.34(d)) shows bigger size grains of iron of size 5-10 μm. Fig. 6.34(e) shows the SEM of the same specimen at 10000X magnification which reveals the strong bonding between the various particles of the constituent phases. This bonding among the various particles is formed due to the deformation process. The last micrograph shows the microscopic image of the specimen at 15000X (Fig. 6.34(f)). The present SEM image reveals no cracks on the inner surface of the specimen.

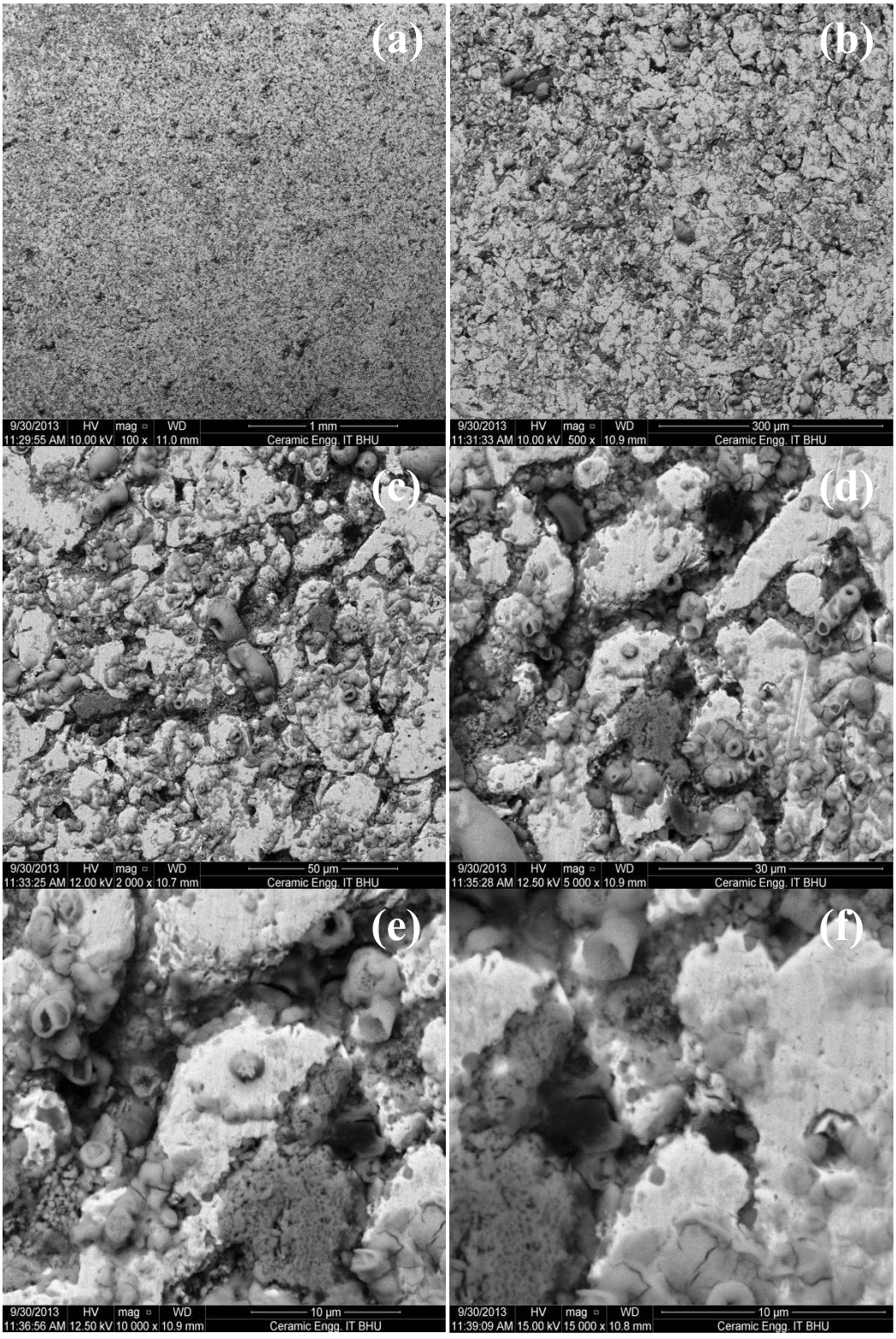

Fig. 6.34 SEM of deformed specimen with h/d<1 in dry state at (a) 100X (b) 500X (c) 2000 X (d) 5000X (e) 10000X and (f) 15000X

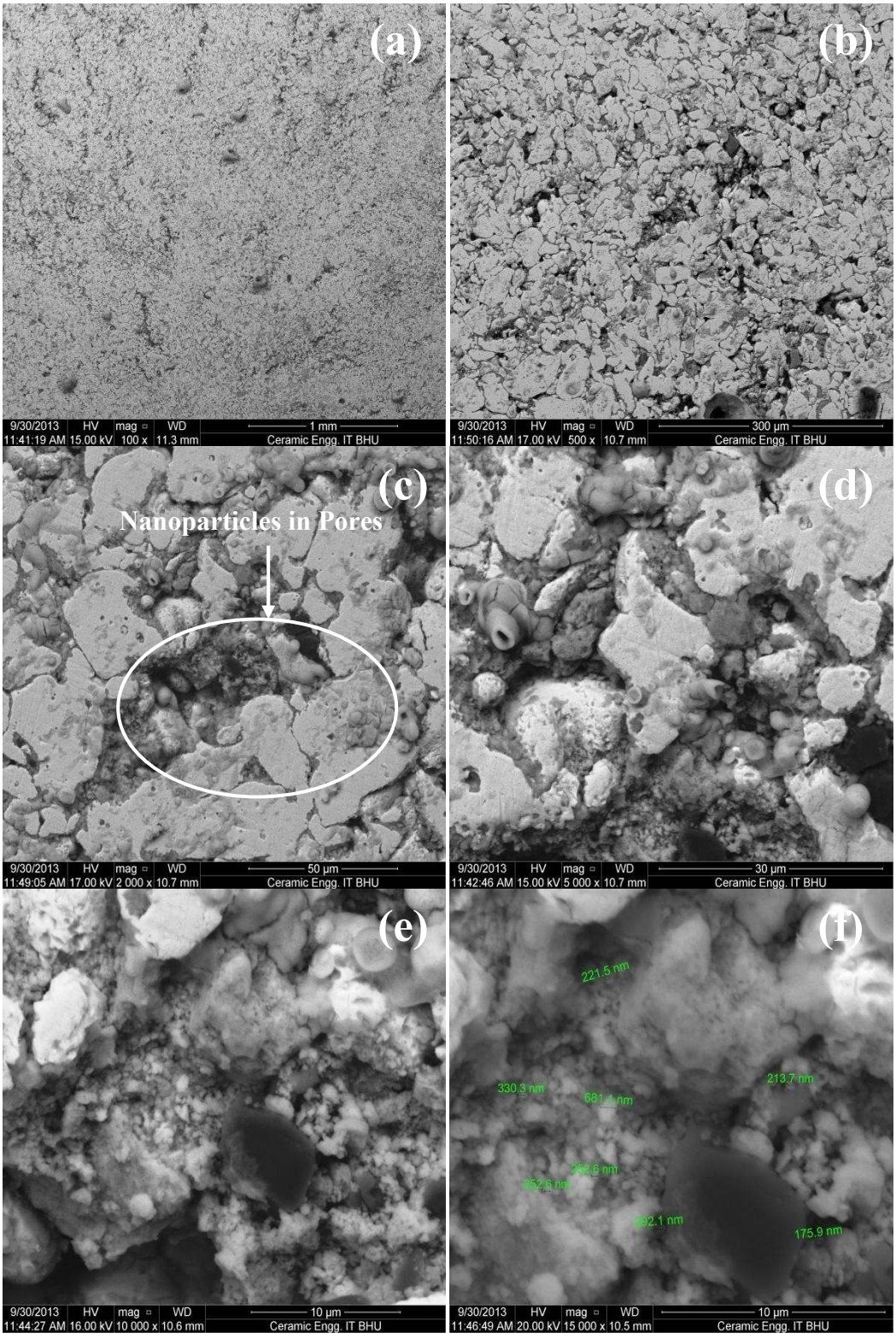

Fig. 6.35 SEM of deformed specimen with h/d<1 in solid lubricating (Graphite Powder) at (a) 100X (b) 500X (c) 2000 X (d) 5000X (e) 10000X and (f) 15000X

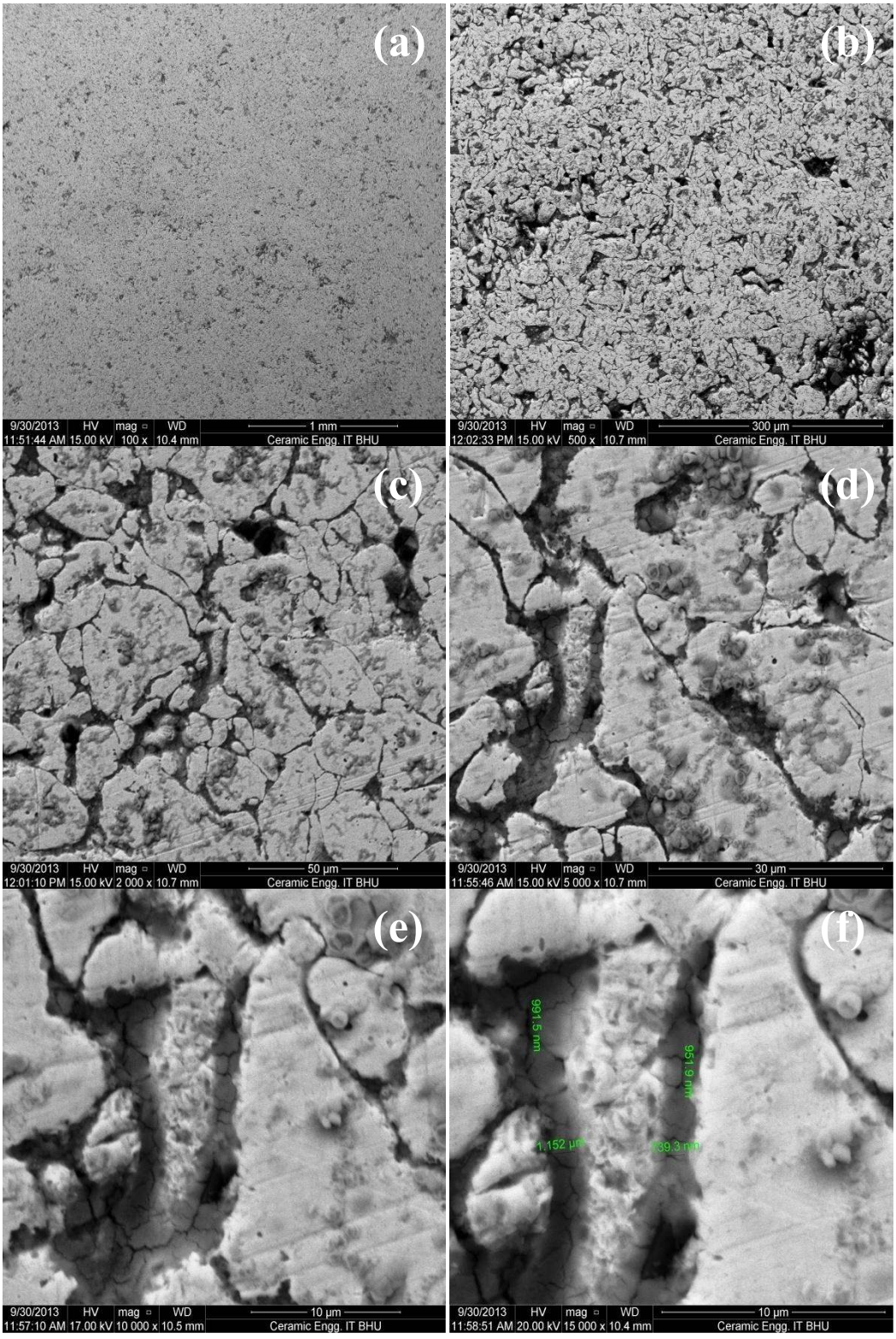

Fig. 6.36 SEM of deformed specimen with h/d<1 in liquid lubricating (Oil) at (a) 100X (b) 500X (c) 2000 X (d) 5000X (e) 10000X and (f) 15000X

Fig. 6.35 shows the SEM of deformed specimen with h/d<1 in solid lubricating, (Graphite Powder) at (a) 100X (b) 500X (c) 2000X (d) 5000X (e) 10000X and (f) 15000X. Fig. 6.35(a) shows the micrograph of the specimen at 100X magnification which shows a highly dense phase structure in comparison with the sintered condition. This micrograph is denser in comparison with the specimen deformed in dry condition. The same micrograph when viewed at 500X magnification (Fig. 6.35(b)) shows a considerable amount of reduction in the intragranular porosity. It also reveals the homogenously distributed grains of constituent phases. Fig. 6.35(c) shows the SEM of the same specimen at 2000X magnification which shows the entrapment of fine nano size iron aluminate particles in the intragranular pores of the specimen. Due to this filling of the nano particles in the pores of the specimen, the specimen achieves much more densification. The same specimen when viewed at 5000X magnification (Fig. 6.35(d)) shows bigger size grains of iron of size 5-10 μm. Fig. 6.35(e) shows the SEM of the same specimen at 10000X magnification which reveals the strong bonding between the various particles of the constituent phases. This bonding among the various particles is formed due to the deformation process. Due to the deformation process the grain interlocking and filling of the pores with the nano size particles can be seen. The last micrograph shows the electron microscopic image of the specimen at 15000X (Fig. 6.35(f)). The present SEM image reveals no cracks on the inner surface of the specimen as well as it shows nano size particles in the range of 200-300 nm respectively.

Fig. 6.36 shows the SEM of the deformed specimen with h/d<1 in liquid lubricating (Oil) at (a) 100X (b) 500X (c) 2000 X (d) 5000X (e) 10000X and (f) 15000X. Fig. 6.36(a) shows the micrograph of the specimen at 100X magnification which shows a highly dense phase structure in comparison with the sintered condition. This micrograph is denser in comparison with the specimen deformed under dry and solid lubricating condition. The same micrograph when viewed at 500X magnification (Fig. 6.36(b)) shows a considerable amount of reduction in the intragranular porosity. Similar to the previous two specimens, this also shows the homogenously distributed grains of constituent phases. Fig. 6.36(c) shows the SEM of the same specimen at

2000X magnification which shows the entrapment of fine nanosizeiron aluminate particles in the intragranular pores of the specimen. Due to this filling of the nano particles in the pores of the specimen, the specimen achieves much more densification. The same specimen when viewed at 5000X magnification (Fig. 6.36(d)) shows bigger size grains of iron of size 5-10 μm. Fig. 6.36(e) shows the SEM of the same specimen at 10000X magnification which reveals the strong bonding between the various particles of the constituent phases. This bonding among the various particles is formed due to the deformation process. The last micrograph shows the microscopic image of the specimen at 15000X (Fig. 6.36(f)). The present SEM image also reveals no cracks on the inner surface of the specimen.

Fig. 6.37 shows the SEM images of deformed specimen with h/d=1 in dry state at (a) 100X (b) 500X (c) 2000X (d) 5000X (e) 10000X and (f) 30000X after cutting the specimen in the transverse direction. The micrograph at 100X [Fig. 6.37(a)] shows a higher density amongst the constituent particles in comparison with the micrographs taken before the deformation. It was also observed that the porosity factor was almost negligible due to the closer coming of the intergranular and intragranular porosity during the deformation process. The same micrograph when viewed at 500X magnification [Fig. 6.37(b)] shows plastically deformed grains of the various constituent phases. These grains severely undergo bonding resulting in strengthening caused by the action of Al_2O_3 reinforcement and by nano size iron aluminate phase. The micrograph of the same specimen at 2000X magnification [Fig. 6.37(c)] shows the conjunction of different particles or flake type arrangement of the constituent phases formed during the plastic deformation of the composites. It was also observed that during the deformation process, each grain is deforming homogenously in conformity with the deformation of the specimen as a whole. This causes constraints imposed by continuity and considerable differences in the deformation between neighboring grain and within each grain. A clear view and justification of this discussion is illustrated in Fig. 6.37(d) which shows the micrograph of the same specimen at 5000X revealing a flake type arrangement of length 5-8 μm and width 10-12 μm along with some nano size grains formed due to the deformation process.

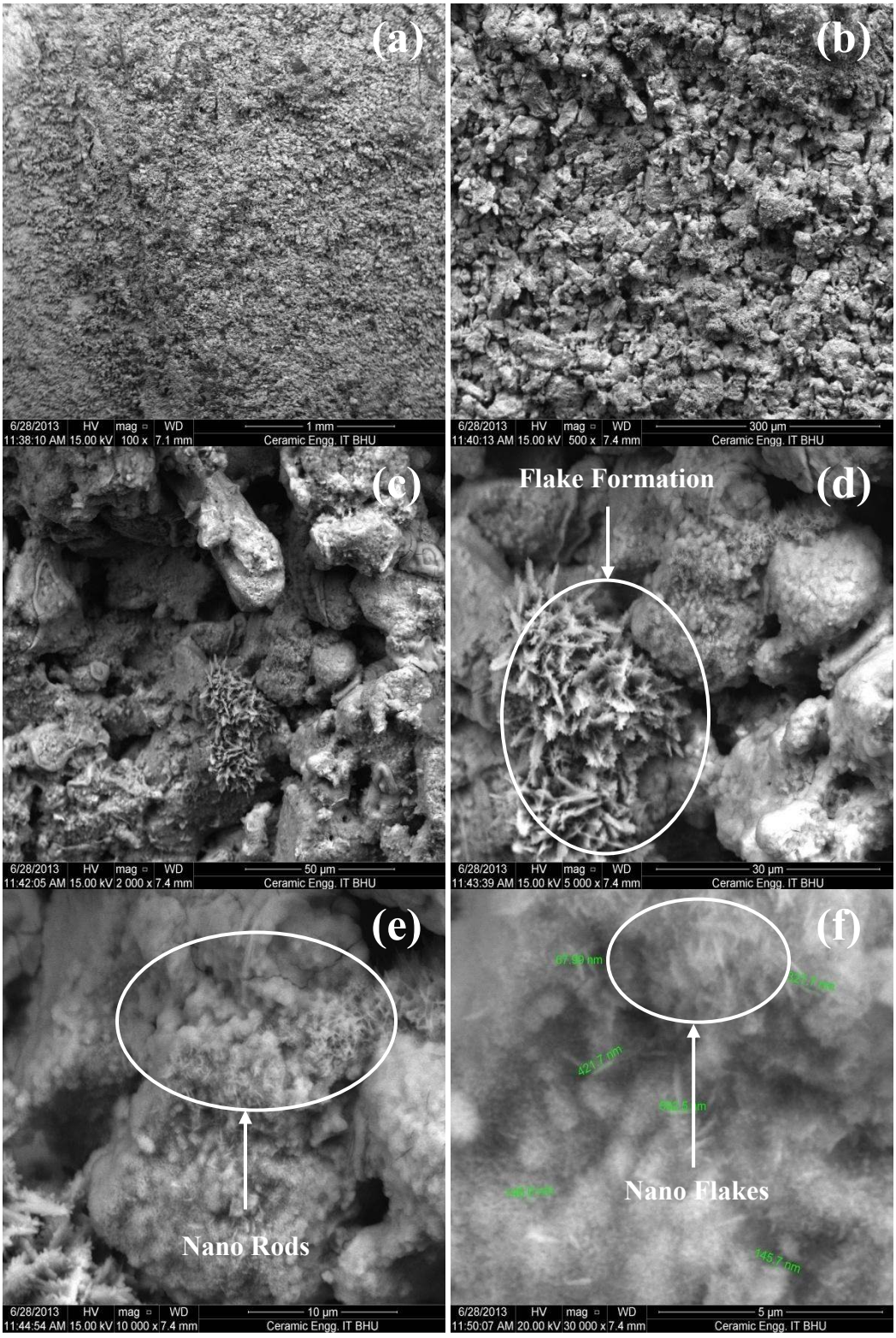

Fig. 6.37 SEM of deformed specimen with h/d=1 in dry state at (a) 100X (b) 500X (c) 2000 X (d) 5000X (e) 10000X and (f) 30000X

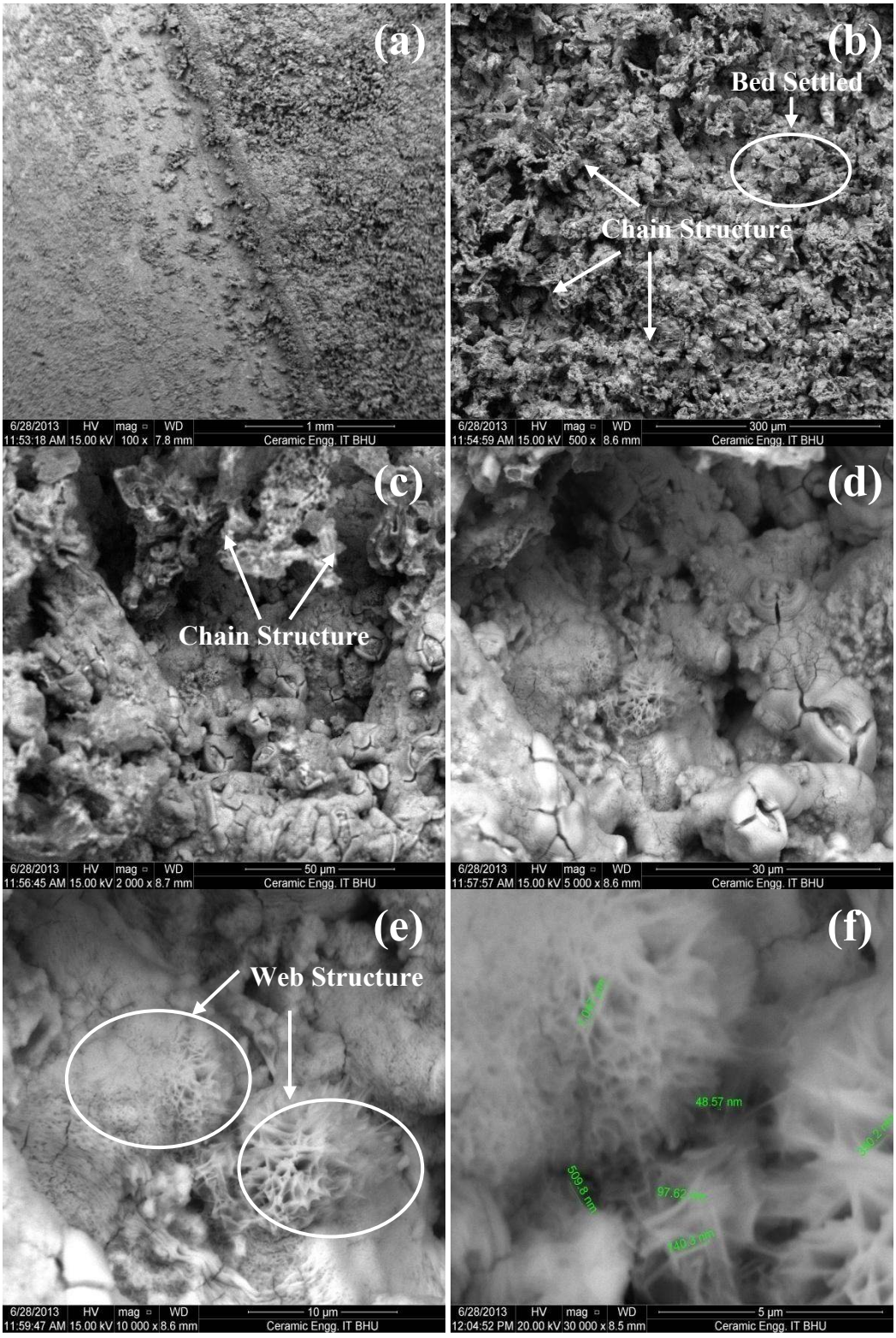

Fig. 6.38 SEM of deformed specimen with h/d=1 in solid lubricating (Graphite Powder) state at (a) 100X (b) 500X (c) 2000 X (d) 5000X (e) 10000X and (f) 30000X

It is also seen that there is a presence of some nano particles on the intraparticles site of the composite structure also. The micrograph of the same specimen at 10000X magnification is shown in Fig. 6.37(e) which illustrates some sub micron size nano rods of iron aluminate phase formed during the deformation process. Lastly, the micrograph at 30000X magnification (Fig. 6.37(f)) illustrates the formation of some nano size rods of length varying from 60-600 nm size range. The same micrograph also illustrates the presence of some nano size particles of iron aluminate.

Fig. 6.38 shows the SEM images of deformed specimen with h/d=1 tested in solid lubricating (Graphite Powder) condition at (a) 100X (b) 500X (c) 2000 X (d) 5000X (e) 10000X and (f) 30000X after cutting the specimen in the transverse direction.The micrograph of the composite specimen at 100X magnification (Fig. 6.38(a)) shows a highly dense phase structure in comparison to the micrograph of the specimen before deformation. Fig. 6.38(b) shows the SEM image of the same specimen at 500X magnification which shows basically two types of grain geometry: (1) Grains settled in a uniform manner and (2) the group of grains which are making a chain type structure amongst one another. These two types of the arrangements are formed due to the plastic deformation of the constituent phases. During the plastic deformation, when the load is removed, some particles remain as they are and some regain their original shape and size thus forming two types of geometries as discussed in point 1 and 2 respectively. An inner view of the settled bed of grains is visible in more detail in Fig. 6.38(c) which shows the micrograph of the same specimen at 2000X. It shows some minute microcracks on the site of the grains. Fig. 6.38(d) shows the SEM of the same specimen at 5000X magnification which shows a highly dense structure of the inner bed settled location having microcracks. Micrographs at 6.38(e) and 6.38(f) show the SEM images of the same specimen at 10000X and 30000X which shows the a web type structure. This web type structure has several threads which are of the iron aluminate phases formed during the deformation process. The effect is quite prominent due to which a large number of nano threads are formed and can be viewed very clearly in the last micrograph.

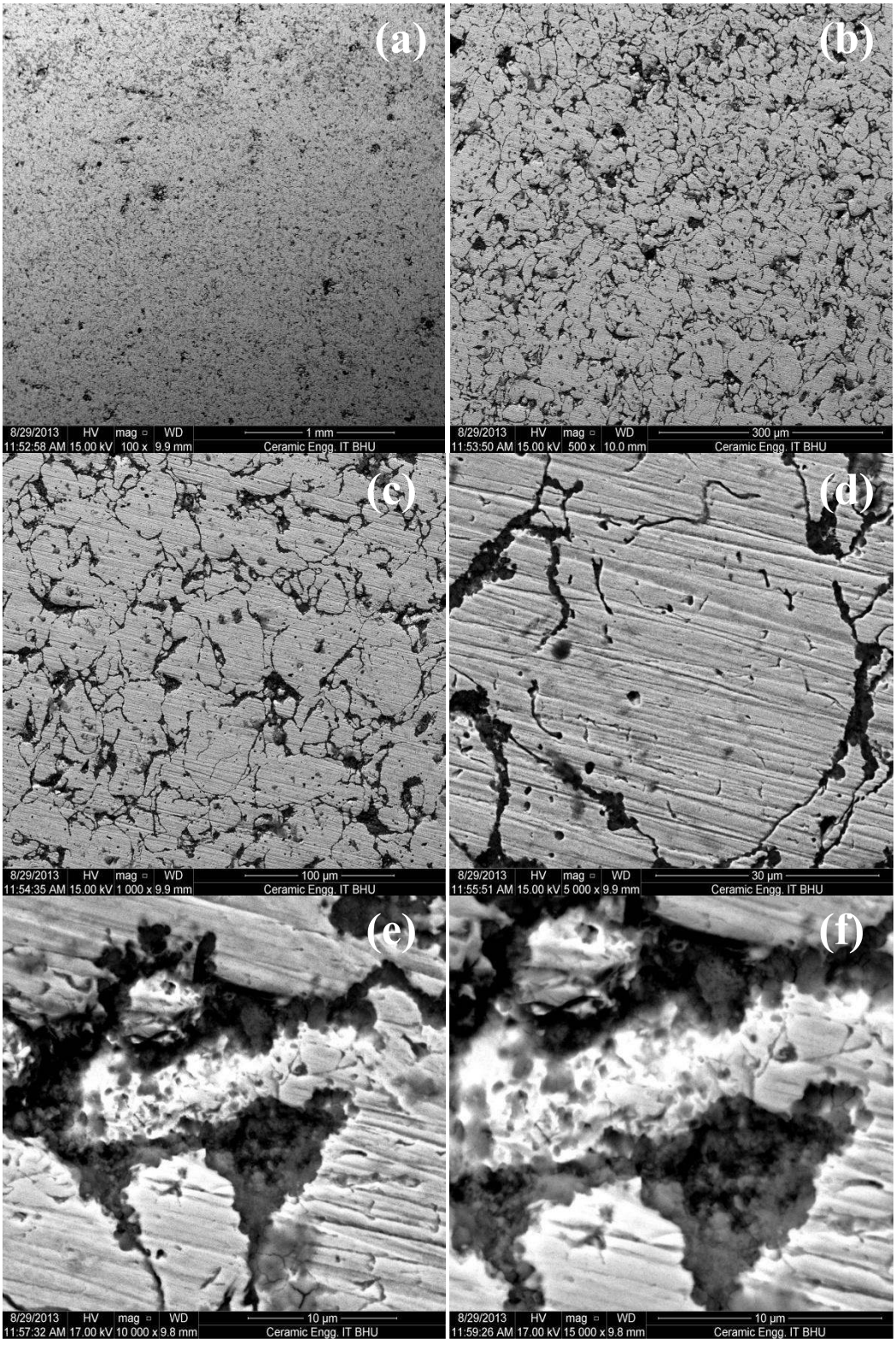

Fig. 6.39 SEM of deformed specimen with h/d>1 in dry state at (a) 100X (b) 500X (c) 1000 X (d) 5000X (e) 10000X and (f) 15000X

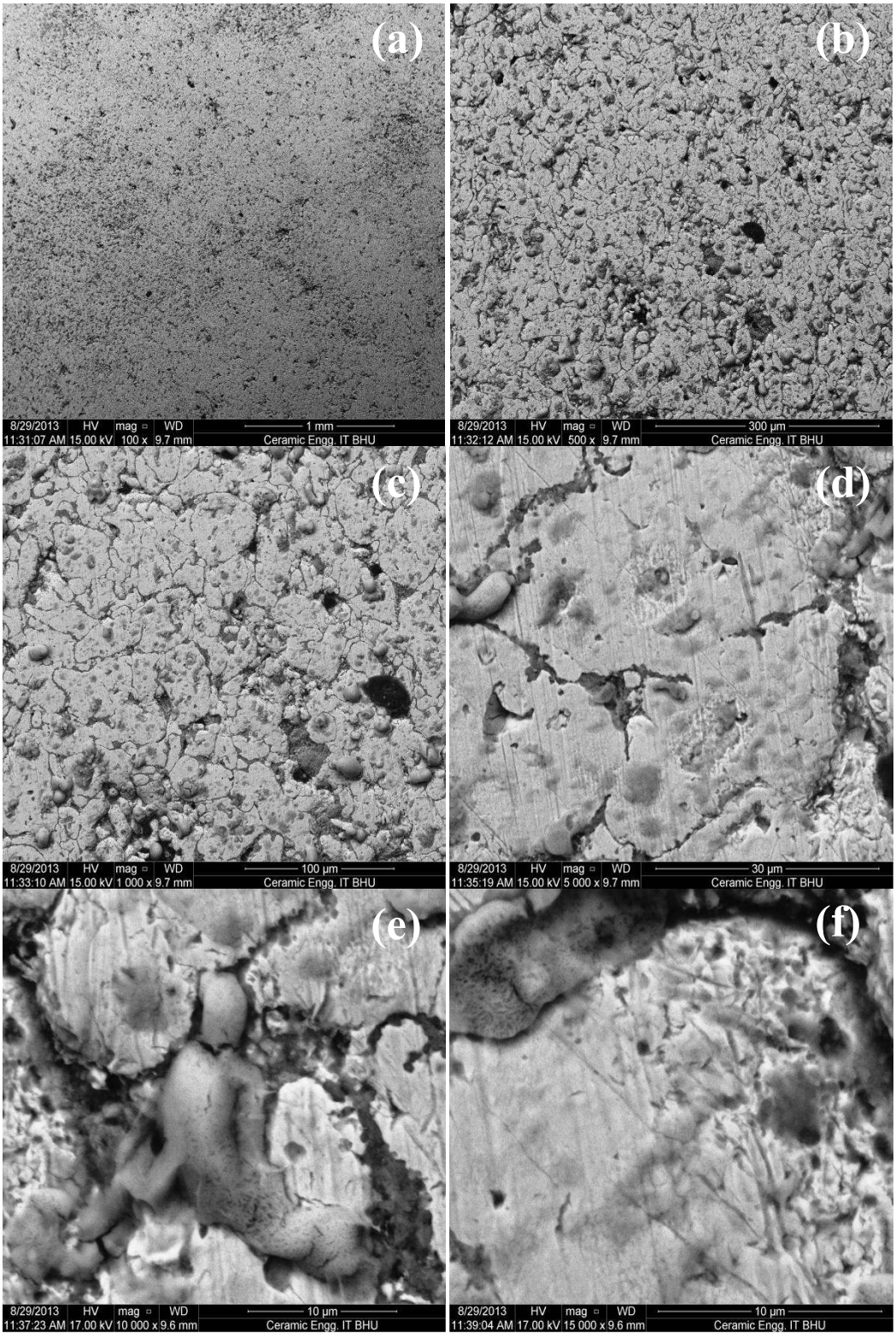

Fig. 6.40 SEM of deformed specimen with h/d>1 in solid lubricating (Graphite Powder) state at (a) 100X (b) 500X (c) 1000 X (d) 5000X (e) 10000X and (f) 15000X

Fig. 6.39 shows the SEM of the deformed specimen with h/d>1 in dry state at (a) 100X (b) 500X (c) 1000 X (d) 5000X (e) 10000X and (f) 15000X respectively. The micrograph at 100X magnification (Fig. 6.39(a)) shows a highly dense phase composite structure having negligible amount of porosity. The micrograph at 500X magnification illustrated in Fig. 6.39(b) shows the closer coming of the intergranular pores which is due to the deformation action. Fig. 6.39(c) shows the same structure when viewed at 1000X magnification reveals that the pores which are present in the grains i.e. intragranular pores are also reduced in size due to the deformation action. The same micrograph when seen at 5000X magnification (Fig. 6.39(d)) shows that there is a formation of some nano size particles of iron aluminate phase on the intragranular sites of the composite specimen. The presence of these nano size particles can be seen much more clearly in the micrographs taken at 10000X (Fig. 6.39(e)) and 15000X (Fig. 6.39(f)) magnification. It could be concluded from the above micrographs that the closer coming of the intergranular and intragranular pores is due to the deformation process. It is also evident that the nano size particles which were subsided in the pores of the specimen moved up to the surface of the nanocomposite specimen after deformation process due to which the various factors such as density and hardness were found to increase. The density and hardness numbers improved as compared with the sintered values.

Fig. 6.40 shows the SEM images of the deformed specimen with h/d>1 under solid lubricating (Graphite Powder) at (a) 100X (b) 500X (c) 1000X (d) 5000X (e) 10000X and (f) 15000X magnification respectively. The micrograph at 100X magnification, Fig 6.40(a) illustrates the formation of dense phase structure with the presence of some small amount of pores. The same micrograph when viewed at 500X magnification (Fig. 6.40(b)) shows a reduction in the amount of pores in comparison to the micrograph taken for sintered specimen. The reduction in the pore size can be attributed due to the deformation action. The same micrograph when viewed at 1000X magnification (Fig. 6.40(c)) reveals that the intergranular as well as the intragranular porosity present on the specimen surface is completely removed due to this deformation process. The higher magnification view of the same specimen at

5000X magnification (Fig. 6.40(d)) reveals the reduction in the grain size. Apart from this, due to the deformation process, not only the grain size reduction takes place but the closer coming of the grains is also taking place. It was very much interesting to note from Fig. 6.40(e) and 6.40(f) that even after the deformation process there was no cracks on the specimen surface.

On the basis of the above results it can be concluded that there is a plastic deformation in the nanocomposite specimens under the action of the compressive stresses. On the basis of compressive stresses, strength of the matrix and bonding strength of the grain boundaries deformation can take place in two types of modes; (a) Grain deformation and (b) Boundary slip. "Grain deformation" occurs when the bonding strength at the boundaries among the metal matrix composite particles exceeds that of the matrix particles and compressive stresses exceeds yield strength of the matrix, i.e. the matrix particles deform plastically first. Second phenomenon is the "boundary slip" which occurs when the bonding strength of the grain boundaries is lower than the strength of the matrix particles. Under compressive loading, when the shear stress exceeds the shear strength of the grain boundaries, then the shear stress induced at the boundaries among the particles causes boundary slip or sliding. Large scoring marks can be seen in the microstructure of the deformed specimens due to the boundary slip [Rabiei et al. (2008)].

In the present case, due to the reactive sintering there is an iron aluminate phase formation which gets deformed and fills in the porosity of the nanocomposite specimens. When the bonding strength between matrix and reinforcement phase is strong and there is also a reactive phase, then by the effect of compressive stresses a strong web and flake type structure is formed. In such type of cases plastic deformation is simultaneously caused by the "boundary slip" and "grain deformation" mechanisms. "Boundary slip" occurs among the reinforcing particles and the matrix particles and "grain deformation" occurs among the reactive particles ($FeAl_2O_4$). Under such conditions, there is an increase in the strength of the composite [Lin et al. (2004)].

The value of stress during the deformation process in all the specimens is found to be highest at the centre and it reduces as it travels towards the outer periphery. In h/d <1 and h/d=1, the value of stress is greater than that of the yield strength value, therefore, there is grain deformation as well as there is grain boundary slipping in the specimens under all the interfacial friction conditions. For h/d>1, the value of stress is less than the yield strength. Therefore there is only boundary slip in the specimen deformed under all the frictional conditions. Microstructures of specimens having h/d<1 and equal to 1 shows the presence of nano iron aluminate phase in the intergranular and intragranular pores of the specimen. Microstructures of specimens having h/d>1, shows the presence of the sliding marks on the specimen surface due to the effect of grain boundary sliding.

6.3.6 Discussion on Theoretical and Experimental Results

Table 6.4 depicts the theoretical and experimental densities of the sintered porous composite samples after compression as determined using different equations given in Chapter 4. For all the samples initial relative density of the composite, ρ_i is taken as 0.7. Yield strength of the composite during compression σ_c is calculated using expression (2) [Chapter 4]. Using the value of σ_c and expression (4.12), Instantaneous relative density of the composite, ρ_{Inst} is calculated. Finally theoretical density d_f is calculated using expression (4.11) [Chapter 4].

Specimen having h/d ratio less than 1 and tested in dry condition showed experimental density as 7.227 gm/cc and theoretical density as 7.155 gm/cc whereas when the same specimen was tested with graphite as lubricant showed experimental density as 7.0454 gm/cc and theoretical density as 6.983 gm/cc however when the same specimen was tested with oil as the lubricant showed the experimental density as 6.710 gm/cc and theoretical density as 6.650 gm/cc. In the similar manner specimen having h/d ratio equal to 1 and tested in dry condition showed experimental density as 6.878 gm/cc and theoretical density as 6.867 gm/cc. When the same specimen was tested with graphite as lubricant showed experimental density as 6.9500 gm/cc and theoretical density as 6.941 gm/cc. When the same specimen was

tested with oil as the lubricant showed the experimental density as 7.628 gm/cc and theoretical density as 7.618 gm/cc.

Table 6.4: Theoretical and Experimental densities of the deformed specimens

Sample no.	ρ_c (gm/cc)	d_{sc} (gm/cc)	ρ_i	η	σ_o (MPa)	p (MPa)	σ_c (MPa)	ρ_{Inst}	d_{exp} (gm/cc)	d_f (gm/cc)
h/d<1 Dry	4.980	7.5	0.7	0.1273	97.30	196.48	63.96	0.9900	7.227	7.155
h/d<1 Grap.	5.011	7.5	0.7	0.1273	97.30	201.45	63.96	0.9911	7.045	6.983
h/d<1 Oil	4.870	7.5	0.7	0.1273	97.30	198.94	63.96	0.9910	6.710	6.650
h/d=1 Dry	4.987	7.5	0.7	0.1273	97.30	275.35	63.96	0.9984	6.878	6.867
h/d=1 Grap.	5.075	7.5	0.7	0.1273	97.30	283.63	63.96	0.9987	6.950	6.941
h/d=1 Oil	4.874	7.5	0.7	0.1273	97.30	283.63	63.96	0.9987	7.628	7.618
h/d>1 Dry	5.115	7.5	0.7	0.1273	97.30	378.49	63.96	0.9998	6.838	6.836
h/d>1 Grap	5.003	7.5	0.7	0.1273	97.30	372.04	63.96	0.9998	6.590	6.589
h/d>1 Oil	4.939	7.5	0.7	0.1273	97.30	372.04	63.96	0.9998	6.934	6.932

The last slot of the specimen was fabricated with h/d ratio as greater than 1, specimen tested with dry condition showed experimental density as 6.838 gm/cc and theoretical density as 6.836 gm/cc, specimens tested with graphite as lubricant showed experimental density as 6.590 gm/cc and theoretical density as 6.589 gm/cc whereas the specimen tested with oil as the lubricant showed experimental density as 6.934 gm/cc and theoretical density as 6.932 gm/cc. From the above discussion it can be concluded that the instantaneous relative density of all the specimen lies in between 0.9900 to 0.9998 and also the theoretical deformed densities of the nanocomposite specimens were in close proximity with that of the experimental results.

The present chapter discussed in detail the wear characterization of Fe-Al_2O_3 metal matrix nanocomposites. The idea of wear testing at varying loads was explored completely in the current chapter. Dry sliding wear test was carried out on the specimens at a load of 0.5, 1.0 and 2.0 kg respectively. Scanning electron

micrographs of the worn out specimens were also taken. The wear rate values and micrograph of worn specimens helped in getting the deeper understanding of the subject. It was found that the wear behavior of the specimens depends on the iron aluminate phase formation. For 5% of Al_2O_3 addition the adhesive wear was more prominent at lower load whereas abrasive wear was more prominent at higher load. For 10% of Al_2O_3 reinforcement the removal of the material is due to fragmentation of asperities and also due to cutting and flowing actions of penetrated hard asperities into the softer surface. It can also be seen from table 6.1 that the wear rate of 5% Al_2O_3 reinforced iron matrix composites showed low values of wear rate at 0.5 kg load whereas the wear rate values were high at higher loads i.e. at 1.0 and 2.0 kg in comparison to 10% Al_2O_3 reinforced iron matrix nanocomposites. Thus, it can be concluded that the wear rate values reduced significantly on increasing the amount of Al_2O_3 reinforcement for higher values of loads.

In the last part of the present chapter specimens having different height to diameter (h/d) ratios have been synthesized by compacting and sintering at 1100°C for 1 h and deformed at room temperatures under different interfacial friction conditions. It is found from the results that the dry specimens show more bulging than the lubricated ones. The test specimen show more surface movement on top surface than the bottom surface under all the deforming conditions. SEM images of h/d<1 showed the crushing action between the grains, h/d=1 shows the grain growth formation in the form of nano flakes and nano rods whereas the h/d> 1 images shows the sliding action between the grain boundaries and grains respectively. Apart from this the present chapter also focuses on the verification of the experimental deformed density with the theoretical deformed density.

The next chapter 7 discusses the effect of CoO and CeO_2 doping on Fe-Al_2O_3 Metal Matrix Nanocomposites synthesized by powder metallurgy. 0.5 and 1.0% of cobalt oxide and cerium oxide was used as the dopant in the present system. XRD, SEM, density, hardness and wear studies of the synthesized nanocomposite specimens were carried out.